IEEE Access
Multidisciplinary ⋮ Rapid Review ⋮ Open Access Journal

Received January 19, 2020, accepted February 1, 2020, date of publication February 10, 2020, date of current version February 18, 2020.

Digital Object Identifier 10.1109/ACCESS.2020.2972570

Analysis and Recovery of Aircraft Deep-Stall Phenomena Using Bifurcation Analysis

DAWEI WU[1], MOU CHEN[2], (Member, IEEE), AND HUI YE[3]

[1]College of Energy and Electrical Engineering, Hohai University, Nanjing 211100, China
[2]College of Automation Engineering, Nanjing University of Aeronautics and Astronautics, Nanjing 211106, China
[3]School of Electronics and Information, Jiangsu University of Science and Technology, Zhenjiang 212003, China

Corresponding author: Mou Chen (chenmou@nuaa.edu.cn)

This work was supported by the Fundamental Research Funds for the Central Universities under Grant 2019B04214.

ABSTRACT In this paper, the problem of deep-stall recovery will be studied for the aircraft without longitudinal static stability. A new longitudinal short-period deep-stall model is established in the presence of time-varying distributed delays. Based on bifurcation analysis method, the effects of actuator fault on deep stall are analyzed in depth. Considering the system uncertainty, actuator fault, input saturation and unsteady disturbance, a finite-time prescribed performance deep-stall recovery law is designed according to the bifurcation analysis results. Further, to avoid the singularity problem in traditional finite-time control, an improved finite-time control law is developed. Stability of the closed-loop system is proved by common Lyapunov functional method. And simulations are given to illustrate the validity of the proposed deep-stall recovery control scheme.

INDEX TERMS Deep stall, finite-time control, prescribed performance, bifurcation analysis.

I. INTRODUCTION

Deep stall is an uncontrollable state. When a fighter enters deep stall, the angle of attack (AOA) increases automatically and will be locked at a certain AOA far beyond the stall AOA [1]. Deep stall widely exists in aircrafts with longitudinal torque characteristics that have a ''spoon-like'' structure, such as the F-16 fighter. Hence, many scholars have deeply studied the deep-stall phenomenon [2]–[4]. In [5], a static deep-stall recovery control law and a dynamic deep-stall recovery control law were discussed for a class of aircrafts with relaxed static stability. In [6], a deep-stall recovery control law was designed based on the bang-bang control method. In addition, the sliding mode control method has also been considered to achieve the deep-stall recovery in [7]. According to [2]–[7], it can be concluded that traditional deep-stall recovery mechanisms are to achieve instability in the deep-stall area and rock the aircraft to overcome the deep-stall attraction.

Different from above studies on deep stall, aircrafts without ''spoon-like'' longitudinal torque characteristics will be studied in this paper. The longitudinal flight dynamics of these aircrafts is statically unstable, and has no stable high AOA open-loop equilibrium area [8]. Hence, the existing deep-stall recovery methods can not be directly adopted in this paper. To analyze the deep-stall phenomenon induced by actuator fault, the bifurcation analysis method will be adopted in this paper. Bifurcation analysis technology has been widely used in the analysis of aircraft dynamic characteristics, and was applied to the design of flight control laws [9]–[11]. In [12], bifurcation analysis method was used to analyze the high AOA characteristics of aircrafts, and some dangerous phenomena can be predicted based on the analysis results, such as departure, deep stall, wing rock, etc. In [13], bifurcation analysis method was used to analyze the maneuverability of the F-18 aircraft, and the analysis results were taken to guide the design of the sliding mode flight controller. In [14], through the bifurcation method, the effects of flexibility on the stability of the aircraft were evaluated. In this paper, the effects of actuator fault on the aircraft stability at high angles of attack will be discussed. And the analysis results show that actuator fault may induce a phenomenon similar to deep stall in the statically unstable aircraft, which has rarely been studied.

For statically unstable aircrafts, a novel finite-time adaptive prescribed performance deep-stall recovery control law will be designed in this paper. In addition to the characteristic of finite-time convergence, the finite-time control system

The associate editor coordinating the review of this manuscript and approving it for publication was Sing Kiong Nguang.

has better robust performance and anti-disturbance performance because of the fractional power term in finite-time controllers. Meanwhile, the prescribed performance control has a satisfactory effect on improving the transient performance and steady-state performance of the system. In [15], the prescribed performance method was first proposed, which can ensure that the constrained variables remain within the preset range. In recent years, the prescribed performance method has been widely studied [16]–[18]. In [19], the prescribed performance method was adopted to design a switched non-strict-feedback nonlinear system control. In [20], the prescribed performance method and fuzzy control were combined. Meanwhile, finite-time control has also been greatly developed [21]–[24]. In [25], a finite-time control was applied in the control of linear parameter-varying systems. In [26], a finite-time trajectory tracking control law was designed for a marine surface vehicle. However, finite-time prescribed performance control has rarely been considered.

Based on the above discussion, a longitudinal attitude model of an aircraft will be established according to the dynamic characteristics of deep stall. Further, the effects of actuator fault on aircraft stability at high angles of attack will be evaluated through the bifurcation analysis method. Then, considering the effects of system uncertainties, unsteady disturbances, actuator fault and input saturation, a finite-time prescribed performance deep-stall recovery law will be designed. Finally, a simulation study is carried out to illustrate the feasibility of the post-stall recovery control scheme, followed by the conclusion. And the main contributions of this paper are as follows:

(1) To describe aerodynamic characteristics of aircrafts at high AOA more accurately, a new deep-stall model is proposed for the first time, which is a non-strict feedback nonlinear system with time-varying distributed delays. The mechanism of deep-stall induced by actuator fault is analyzed in detail, and the corresponding deep-stall recovery scheme is designed according to the analysis results.
(2) To improve the performance of deep-stall recovery, finite-time control and prescribed performance control are combined to realize the deep-stall recovery law. It has rarely been studied that finite-time control and prescribed performance control are combined and applied to non-strict feedback nonlinear systems with time-varying distributed delays.
(3) To handle controller singularity problem in traditional finite-time control, an improved finite-time control law is developed by introducing a non-smooth term, which changes the closed-loop system into a switched system. Then, finite-time stability of the closed-loop system is proved by common Lyapunov functional method.
(4) The non-strict feedback time-varying distributed delay term is introduced into the post stall model, in which some complicated and challenging issues including system uncertainties, actuator fault and input saturation are addressed. Based on the neural network technology and a variable separation method, a robust finite-time prescribed performance deep-stall recovery law is developed.

II. PROBLEM FORMULATION

A. PROBLEM STATEMENT

In the deep-stall region, the flight speed and trajectory angle do not change much. Therefore, the longitudinal short-period motion equation can be used to describe the deep-stall characteristics [27]:

$$\begin{aligned}\dot{\alpha} &= f_1(\alpha) + \Delta f_1(\alpha) + q + H_1(\alpha, q, t)\\ \dot{q} &= \frac{1}{I_y} Q_{air} S \bar{c} C_m(\alpha, q, \delta_c) + \Delta f_2(\alpha, q)\\ &\quad + \rho g_2' \delta_z(u_z) + H_2(\alpha, q, t)\end{aligned} \tag{1}$$

where α is the AOA. q is the pitching rate. $f_1(\alpha)$ is the known nonlinear function of α. $C_m(\alpha, q, \delta_c)$ is the pitching moment aerodynamic coefficient. Q_{air} is the dynamic pressure. S is the reference surface area of the wing. I_y is the moment of inertia. $\bar{c}$ is the mean aerodynamic chord, and δ_c is the defection of canard. $\Delta f_1(\alpha)$, $\Delta f_2(\alpha, q)$ are unknown nonlinear functions. $g_2' > 0$ is the control gain, which is a known constant. $H_1(\alpha, q, t)$ and $H_2(\alpha, q, t)$ are unsteady disturbances, and will be described later. ρ is the actuator fault signal, which can be written as [28]

$$\rho = \begin{cases} 1, & t < T_\rho \\ \varepsilon_\rho, & t \geq T_\rho \end{cases} \tag{2}$$

where $0 < \varepsilon_\rho < 1$ is an unknown constant, T_ρ is the occurring time of actuator fault. It is worth noting that the smaller the value of ρ is, the more serious the actuator failure is.

At high AOA, the control performance of the canard is almost lost. Hence, the canard is generally fixed, and only the thrust vectoring angle $\delta_z(u_z)$ will be used as the controller, which is subject to saturation constraint described as (3).

$$\delta_z(u_z) = sat(u_z) = \begin{cases} sign(u_z) M_{\delta z}, & |u_z| > M_{\delta z} \\ u_z, & |u_z| \leq M_{\delta z} \end{cases} \tag{3}$$

where $u_z(t) \in R$ is the designed control input. $M_{\delta z} = 15°$ represents the maximum deflection angle of the normal thrust vector.

Due to the complex aerodynamic mechanism of unsteady disturbance, the influence of unsteady disturbance on the deep-stall recovery is seldom considered in the existing research [2]–[4]. Different from previous studies, the concept of time-varying distributed delay is adopted to analyze the effect of unsteady disturbance on aircraft motion [29]:

$$\begin{aligned} H_1(\alpha, q, t) &= \int_{t-\tau_1(t)}^{t} h_1(\alpha(s), q(s))\, ds \\ H_2(\alpha, q, t) &= \int_{t-\tau_2(t)}^{t} h_2(\alpha(s), q(s))\, ds \end{aligned} \tag{4}$$

where $h_i(\alpha, \beta)$ is an unknown smooth function of α and q, $\tau_i(t)$ denotes the unknown time-varying delay, $i = 1, 2$.

The pitching moment aerodynamic coefficient $C_m(\alpha, q, \delta_c)$ can be expressed as [8]:

$$C_m = C_{m0}(\alpha) + C_{mq}(\alpha)\frac{q\bar{c}}{2V} + C_{m\delta_c}(\alpha)(\delta_c - \delta_{c0}(\alpha)) \quad (5)$$

where $C_{m0}(\alpha)$ is the static pitching moment coefficient, $C_{mq}(\alpha)$ and $C_{m\delta_c}(\alpha)$ are the pitching moment coefficients due to the pitching rate and the elevator deflection. V is the airspeed, and $\delta_{c0}(\alpha)$ is a nonlinear function of α.

Remark 1: It is noteworthy that the existence of unsteady disturbances $H_1(\alpha, q, t)$, $H_2(\alpha, q, t)$ transforms system (1) into a nonstrict-feedback system. Therefore, the deep stall recovery considered in this paper will be faced with greater challenges.

B. PRESCRIBED PERFORMANCE

In [15], the prescribed performance method was proposed, which ensures that the constrained output tracking error $e(t) \in R$ remains within a predetermined range. And the idea of prescribed performance method can be expressed by the following inequality:

$$e_l(t) < e(t) < e_u(t) \quad (6)$$

where $e_l(t), e_u(t)$ are the designed lower boundary and upper boundary of the tracking error $e(t)$, respectively. And $e_l(t)$, $e_u(t)$ can be designed based on the following definition:

Definition 1 [15], [30]: A smooth bounded function $b(t) : R^+ + \{0\} \to R^+$ will be called a performance function, if $b(t)$ is decreasing, $|e(0)| < b(0)$ and $\lim_{t\to\infty} b(t) = b_\infty > 0$.

According to Definition 1, the performance function is usually designed as

$$b(t) = (b(0) - b(\infty))e^{-lt} + b(\infty) \quad (7)$$

where $b(0)$ and $b(\infty)$ are design constants, and satisfy $b(0) > b(\infty)$. $l > 0$ is a constant to be designed.

Hence, according to (7), $e_l(t)$, $e_u(t)$ can be chosen as follows:

$$\begin{aligned} e_l(t) &= -Qb(t), e_u(t) = b(t), \quad when\ e(0) \geq 0 \\ e_l(t) &= -b(t), e_u(t) = Qb(t), \quad when\ e(0) < 0 \end{aligned} \quad (8)$$

where $0 < Q \leq 1$ is a design constant.

Thus, invoking (7) and (8), it is obvious that we can adjust the steady-state value and the maximum overshoot of the tracking error $e(t)$ by selecting appropriate values of parameters $b(\infty)$ and $b(0)$. Meanwhile, the parameter l decides the slowest convergence rate of the tracking error.

To achieve the prescribed performance control, we do the following variable transformation:

$$\begin{aligned} e(t) &= ST(\varpi, e_l(t), e_u(t)) \\ \varpi &= ST^{-1}(e(t), e_l(t), e_u(t)) \end{aligned} \quad (9)$$

where ϖ is a new unconstrained error signal. The function $ST(\varpi, e_l(t), e_u(t))$ is a strictly increasing function of the error signal ϖ, and satisfies the following equations:

$$\begin{aligned} \lim_{\varpi\to+\infty} ST(\varpi, e_l(t), e_u(t)) &= e_u(t) \\ \lim_{\varpi\to-\infty} ST(\varpi, e_l(t), e_u(t)) &= e_l(t) \end{aligned} \quad (10)$$

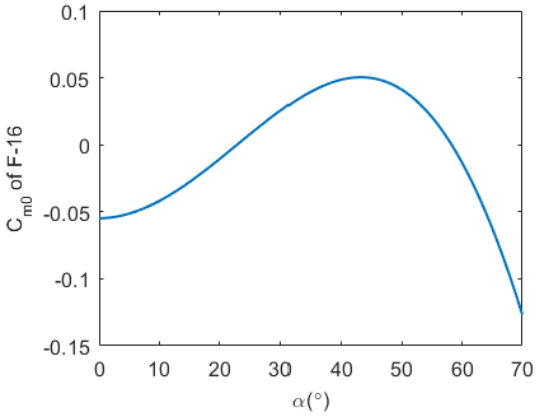

FIGURE 1. The static pitching momentcoefficient of F-16 aircraft.

III. BIFURCATION ANALYSIS OF DEEP STALL

Bifurcation analysis is a powerful analysis method of complex nonlinear system, which can predict the global dynamic characteristics of nonlinear dynamic systems [12]. In this section, the mechanism of deep stall induced by actuator failure will be analyzed in detail through bifurcation analysis method.

Static pitching moment coefficient $C_{m0}(\alpha)$ determines the longitudinal aerodynamic characteristics of an aircraft. The deep-stall phenomenon is widespread in aircrafts with static pitching moment coefficient that has a "spoon-like" structure [7]. Taking the F-16 aircraft as an example, its static pitching moment coefficient is shown in Fig. 1. When $\alpha \leq 44°$, the aircraft is statically unstable. However, when $\alpha > 44°$, the aircraft is statically stable. It is worth noting that this aircraft has a stable equilibrium at high AOA. As a result, the aircraft is very easy to be locked at this point, which forms deep stall.

In this paper, another type of aircrafts will be studied, whose longitudinal moment characteristics have no "spoon-like" structure. Taking the X-31 aircraft as an example, its static pitching moment coefficient is shown in Fig. 2. It is worth noting that this aircraft is statically unstable and has no stable high AOA area. Hence, traditional open-loop bifurcation analysis is not suitable for this aircraft. Then, the closed-loop bifurcation analysis will be adopted in this paper, and the effects of actuator fault on the aircraft stability at high angles of attack will be evaluated.

To perform closed-loop bifurcation analysis on system (1), the unsteady disturbances $H_1(\alpha, q, t)$ and $H_2(\alpha, q, t)$ can be ignored. Because the unsteady disturbances $H_1(\alpha, q, t)$ and $H_2(\alpha, q, t)$ will not affect the steady-state solution of the closed-loop system, and ignoring unsteady disturbances does not affect the bifurcation analysis results. Hence, the nominal

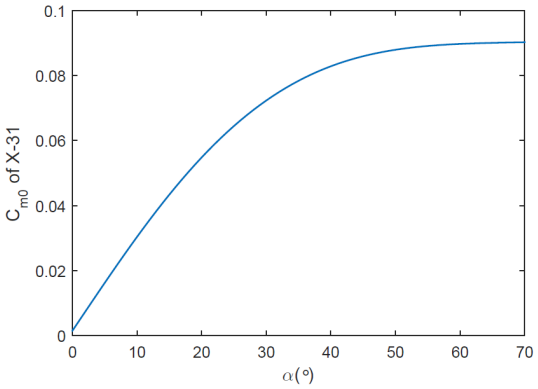

FIGURE 2. The static pitching momentcoefficient of X-31 aircraft.

analytical model of (1) can be written as

$$\begin{aligned}\dot{\alpha} &= f_1(\alpha) + q \\ \dot{q} &= \frac{1}{I_y} QS\bar{c}C_m(\alpha, q, \delta_c) + \rho g_2' \delta_z(u_z)\end{aligned} \tag{11}$$

For the closed-loop bifurcation analysis, the traditional backstepping method is adopted, which has been widely used in the flight control law design [46]–[48]. Based on (11), the backstepping flight control law is designed as

$$\begin{aligned}q_c &= -f_1(\alpha) + \alpha_c - k_{1b}e_{1b} \\ u_z &= -g_2^{'-1}\begin{pmatrix} \frac{QS\bar{c}(C_{m0}(\alpha)}{I_y} + \frac{q\bar{c}C_{mq}(\alpha)}{2V} \\ +k_{2b}e_{2b} - \dot{q}_c + e_{1b} \\ +C_{m\delta_c}(\alpha)(\delta_c - \delta_{c0}(\alpha)) \end{pmatrix}\end{aligned} \tag{12}$$

where α_c is a designed AOA command. $e_{1b} = \alpha - \alpha_c$, $e_{2b} = q - q_c$. $k_{1b} > 0$ and $k_{2b} > 0$ are design constants. Stability of the closed-loop system (11) and (12) can be easily verified. It will not be repeated here. It is worth noting that, in the design of controller (12), the input saturation is not considered. The input saturation will be treated as an input constraint in the bifurcation analysis program.

In general, an aircraft equipped with the thrust vector is difficult to enter deep stall. However, if the aircraft is subjected to strong gust disturbances and the engine thrust is reduced, the aircraft may enter the following dangerous state: $V = 34.9912\ m/s$, $\gamma = -13.6536°$, $\alpha = 50.0364°$, $q = 0°/s$, and $T = 51815\ N$. In this case, if the engine's performance deteriorates, the aircraft will enter a more dangerous state. Hence, in this section, we will take the above state as the initial flight state, the AOA command α_c will be treated as the bifurcation parameter, and the influence of the actuator fault ρ on the the steady-state solution of (11) and (12) will be studied based on the bifurcation method. The analysis results are given in Fig. 3 - Fig. 6.

In Fig. 3 - Fig. 6, the solid blue line indicates the stable equilibrium solution, and the red dashed line represents an unstable equilibrium solution. Fig. 3 shows that the aircraft can achieve a good AOA tracking performance in the absence of actuator fault ($\rho = 1$). When $0.5 < \rho < 1$, the aircraft still has enough control energy to achieve better AOA tracking performance, and the closed-loop bifurcation analysis result is similar to Fig. 3. When $\rho \leq 0.5$, the closed-loop bifurcation analysis results are given in Fig. 4 - Fig. 6. In Fig. 4, when $\rho = 0.44$, the aircraft can achieve small AOA tracking ($0 \leq \alpha_c \leq 48°$). Once the AOA of the aircraft is slightly greater than 48°, the AOA will deviate uncontrollably to

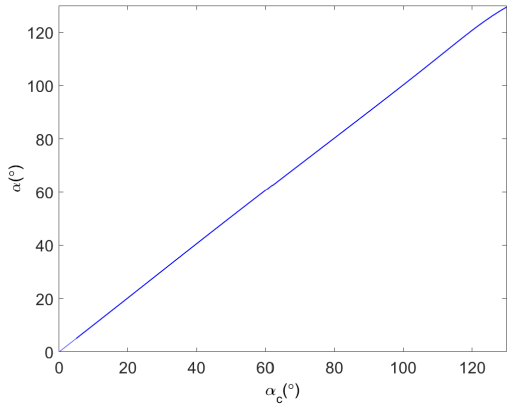

FIGURE 3. $\rho = 1$.

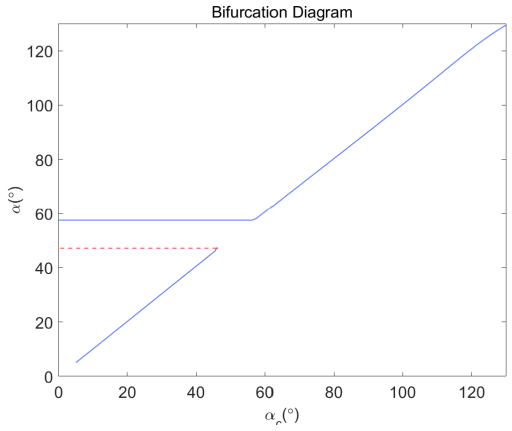

FIGURE 4. $\rho = 0.44$.

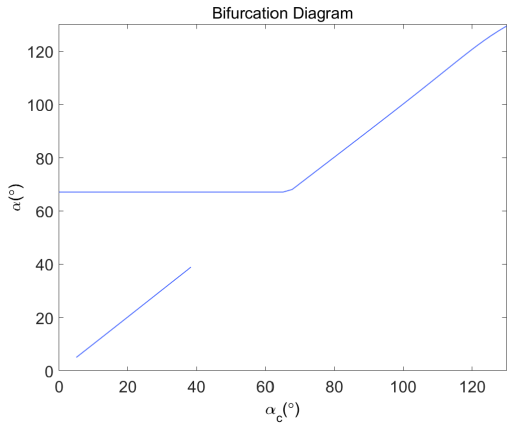

FIGURE 5. $\rho = 0.4$.

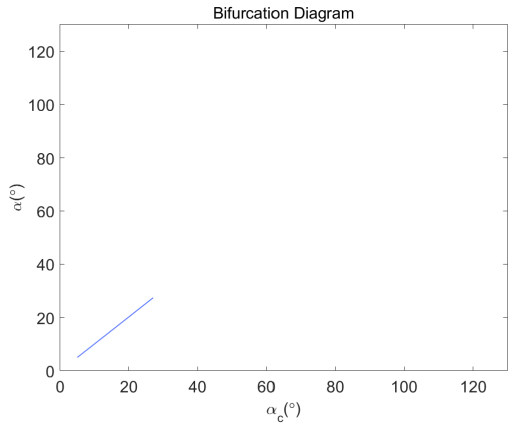

FIGURE 6. $\rho = 0.3$.

a higher AOA (about 58°), and we call this AOA as the deep-stall AOA. It is noteworthy that in this case, even if the AOA command (α_c) is reduced, the aircraft's AOA cannot be restored to a small AOA. However, it is worth noting that if the AOA command α_c is increased, the aircraft can still achieve high AOA tracking. Fig. 5 is similar to Fig. 4, but the deep-stall AOA increases to 68°. Fig. 6 indicates that when control efficiency is further reduced, the aircraft can only achieve small AOA tracking.

Inspired by the analysis results in Fig. 4 and Fig. 5, although the aircraft does not have enough nose down pitching moment, it can still track the high AOA command. Hence, the deep-stall recovery plan is designed as:

(1) First, when the deep stall occurs, a high AOA tracking controller will be activated to increase the AOA of the aircraft.
(2) Then, when the AOA is increased to a specified AOA, the pilot will immediately push the longitudinal stick to force the airplane to pitch down quickly.

To achieve the above deep-stall recovery mechanism, the following assumptions and lemmas are required:

Assumption 1 [31]: For the unknown time-varying delays $\tau_i(t)$ in (4), there are positive constants $\bar{\tau}_i$ and $\bar{\tau}_i^*$, such that $\tau_i(t) \leq \bar{\tau}_i$, $|\dot{\tau}_i(t)| \leq \bar{\tau}_i^* < 1$, $i = 1, 2$.

Assumption 2 [29]: For unknown function $h_i(\alpha, \beta)$ in (4), there exists a strictly increasing smooth function $N_i(\bullet) : R^+ \to R^+$ with $N_i(0) = 0$ such that $h_i^2(x) \leq N_i(\|x\|)$, with $x = [\alpha, \beta]^T$, $i = 1, 2$.

Lemma 1 [32], [33]: For $Z \in \Omega_Z \subset R^p$, any continuous function $f(Z) : R^p \to R$ can be approximated by the output $W^T S(Z)$ of a radial basis function neural network (RBFNN), where Ω_Z is an allowable set of the state vector Z; $W \in R^{p_1}$ is the weight vector; $S(Z) = \left[s_1(Z), s_2(Z), \cdots, s_{p_1}(Z)\right]^T \in R^{p_1}$ is the basis function; p_1 is the designed RBFNN node number. Usually, the basis function is chosen as

$$s_i(Z) = \exp\left[-\frac{(Z-\mu_i)^T(Z-\mu_i)}{\eta^2}\right], i = 1, 2, \ldots, p_1 \tag{13}$$

where $\mu_i = \left[\mu_{i1}, \mu_{i2}, \cdots, \mu_{ip_1}\right]^T$ and η are the center of respective field and the width of the Gaussian function, respectively.

Then, for any given small constant $\bar{\bar{\varepsilon}}$, if p_1 is large enough, we can obtain

$$\begin{aligned} f(Z) &= W^{*T} S(Z) + \bar{\varepsilon}^* \\ \left|\bar{\varepsilon}^*\right| &\leq \bar{\bar{\varepsilon}} \end{aligned} \tag{14}$$

where W^* is the optimal weight value, and $\bar{\varepsilon}^*$ is the optimal bounded approximation error.

Lemma 2 [34]: For $\bar{x}_k = [x_1, \cdots, x_k]^T \in R^k$, $S(\bar{x}_k) = [s_1(\bar{x}_k), \cdots, s_l(\bar{x}_k)]^T$ denotes the basic function vector of an RBFNN. Then, for any two positive integers k and k', if $k' \leq k$, we have

$$\|S(\bar{x}_k)\|^2 \leq \|S(\bar{x}_{k'})\|^2. \tag{15}$$

Lemma 3 [35]: For any constant $b > 0$ and variable z, the following inequation is guaranteed:

$$0 < |z| - z\tanh\left(\frac{z}{b}\right) \leq b\xi \tag{16}$$

where $\xi = 0.2785$ is a constant.

Lemma 4 [31]: If $\Psi > 0$ is a constant matrix, c, d are scalars and satisfy $c < d$, Then, for any vector function $\omega(s) : [c, d] \to R^n$, we have

$$\begin{aligned} &\left(\int_c^d \omega^T(s)\,ds\right)\Psi\left(\int_c^d \omega^T(s)\,ds\right) \\ &\qquad \leq (d-c)\int_c^d \omega^T(s)\,\Psi\omega(s)\,ds \end{aligned} \tag{17}$$

Lemma 5 [32]: For some class K functions $\pi_1 : R \to R$ and $\pi_2 : R \to R$, some positive constants κ and c, if we can find a C^1 continuous and positive-definite Lyapunov function $V(x)$ satisfying $\pi_1(\|x\|) \leq V(x) \leq \pi_2(\|x\|)$ and $\dot{V}(x) \leq -\kappa V(x) + c$, then the solution $x(t)$ is uniformly bounded under bounded initial conditions.

Lemma 6 [36]: For any real variable x_1 and x_2, the following inequality is guaranteed:

$$|x_1|^{c_1}|x_2|^{c_2} \leq \frac{c_1}{c_1+c_2}c_3|x_1|^{c_1+c_2} + \frac{c_2}{c_1+c_2}c_3^{-\frac{c_1}{c_2}}|x_2|^{c_1+c_2} \tag{18}$$

where $c_1 > 0$, $c_2 > 0$ and $c_3 > 0$ are constants.

Lemma 7 [37]: Consider a nonlinear system $\dot{x} = f(x)$. Suppose that there exist a smooth positive definite function $V(x)$ and some positive constants c_4, c_5 and $0 < \lambda_L < 1$ such that

$$\dot{V}(x) \leq -c_4 V^{\lambda_L}(x) + c_5 \tag{19}$$

then the nonlinear system is semiglobal practical finite-time stable (SGPFS).

Remark 2 [38]–[40]: $N_i(\bullet)$ is a strictly increasing function, which makes $N_i\left(\sum_{i=1}^n a_i\right) \leq \sum_{i=1}^n N_i(na_i)$ guaranteed if $a_i \geq 0$, for $i = 1 \cdots n$. Meanwhile, $N_i(s)$ is a smooth

function with $N_i(0) = 0$. Then, a smooth function $\bar{N}_i(s)$ can be found such that $N_i(s) = s\bar{N}_i(s)$, which results in $N_i\left(\sum_{i=1}^{n} a_i\right) \leq \sum_{i=1}^{n} N_i(na_i) = \sum_{i=1}^{n} na_i\bar{N}_i(na_i)$.

Remark 3: In [41], [42], Interval Type-2 Fuzzy Neural Network has been studied and applied to the uncertain processing of hypersonic flight vehicle flight control. In [43], the reentry vehicle control with actuator faults, control delay, input saturation, time-varying parameter uncertainties and external disturbances was studied, and the stability of proposed controller was proved through the linear matrix inequality method. There exists two main differences between this paper and literatures [41]–[43]. On the one hand, different control problem was considered in this paper. According to the characteristics of deep stall, a non-strict feedback nonlinear system is studied in the presence of system uncertainty, actuator failure, distributed time delay and input saturation. On the other hand, finite-time control and prescribed performance control are combined, and the stability was proved based on Lemma 5, Lemma 6, and Lemma 7.

IV. ATTITUDE CONTROLLER DESIGN

According to the deep-stall recovery mechanism, the core of deep-stall recovery is the attitude control at high AOA. Hence, in this section, finite-time control and prescribed performance control will be combined to realize the high AOA attitude controller design. Meanwhile, to solve the problem of controller singularity in traditional finite-time control, an improved finite-time control law is developed by introducing non-smooth terms, which will transform the closed-loop system into a switched system. At last, finite-time stability of the closed-loop system will be proved by common Lyapunov functional method.

Define the following error variables:

$$\begin{aligned} e_1 &= \alpha - \alpha_c \\ e_2 &= q - q_c \end{aligned} \tag{20}$$

where α_c is the given AOA command. q_c is the virtual control law, and will be designed later.

To achieve prescribed performance control, a new variable ϖ_1 will be introduced, which can be obtained from the following equation:

$$e_1 = \frac{e_u - e_l}{\pi}\arctan(\varpi_1) + \frac{e_u + e_l}{2} \tag{21}$$

Based on (21), we obtain the following fact:

$$g_1 = \frac{\partial \varpi_1}{\partial e_1} = \frac{\pi}{e_u - e_l}\cos\left(\frac{\pi}{2} \times \frac{2e_1 - e_u - e_l}{e_u - e_l}\right)^{-2} > 0 \tag{22}$$

Invoking (1) and (22), we have

$$\begin{aligned} \dot{\varpi}_1 &= \frac{\partial \varpi_1}{\partial e_1}\dot{e}_1 + \frac{\partial \varpi_1}{\partial e_u}\dot{e}_u + \frac{\partial \varpi_1}{\partial e_l}\dot{e}_l \\ &= g_1\left(f_1(\alpha) + \Delta f_1(\alpha) + q + H_1(\alpha, q, t) - \dot{\alpha}_c\right) \\ &\quad + N(e_1, e_u, e_l) \end{aligned} \tag{23}$$

where $N(e_1, e_u, e_l) = \frac{\partial \varpi_1}{\partial e_u}\dot{e}_u + \frac{\partial \varpi_1}{\partial e_l}\dot{e}_l$.

According to [45], the following smooth function will be used to handle the input saturation (3):

$$T_{tanh}(u_z) = \delta_M \frac{e^{\frac{u_z}{M_{\delta z}}} - e^{-\frac{u_z}{M_{\delta z}}}}{e^{\frac{u_z}{M_{\delta z}}} + e^{-\frac{u_z}{M_{\delta z}}}} = \left.\frac{\partial T(u_z)}{\partial u_z}\right|_{u_z = u'} u_z \tag{24}$$

where $u' = \mu u_z$, $0 < \mu < 1$.

Substituting (24) into (1), the angular rate equation can be rewritten as

$$\begin{aligned} \dot{q} &= f_2 + \rho g'_2 T_{tanh}(u_z) + \rho g'_2 \zeta(u_z) + H_2(\alpha, q, t) \\ &= f_2 + g_2 u_z + \rho g'_2 \zeta(u_z) + H_2(\alpha, q, t) \end{aligned} \tag{25}$$

where $g_2 = \rho g'_2 \left.\frac{\partial T_{tanh}(u_z)}{\partial u_z}\right|_{u_z = u'} > \sigma > 0$, $f_2 = \frac{1}{I_y} Q_{air} S \bar{c} C_m(\alpha, q, \delta_c)$, and σ is an unknown constant. $\zeta(u_z) = \delta_z(u_z) - T_{tanh}(u_z)$. And it can be proved that there exists a known positive constant M_ξ such that $|\zeta(u_z)| = |\delta_z(u_z) - T_{tanh}(u_z)| \leq M_\zeta$.

Combining (23) and (25), (1) can be transformed into the following system:

$$\begin{aligned} \dot{\varpi}_1 &= g_1(f_1 + \Delta f_1 + q + H_1 - \dot{\alpha}_c) + N \\ \dot{q} &= f_2 + \Delta f_2 + g_2 u_z + \rho g'_2 \zeta(u_z) + H_2 \end{aligned} \tag{26}$$

For (26), the controller will be designed in the following:

$$\begin{aligned} q_c &= -g_1^{-1}\begin{pmatrix} k_{11}\varpi_1 + k_{12}\psi_{11}(\varpi_1) + \frac{\varepsilon_{11}}{2}\varpi_1 \bar{f}_1^2 \\ + \frac{1}{2}\varpi_1 g_1^2 + \hat{\theta}_{12}\tanh\left(\frac{\varpi_1}{b_1}\right) \\ + \frac{\varepsilon_{13}}{2}\varpi_1 \hat{\theta}_{11} S_1^T(Z_1) S_1(Z_1) \end{pmatrix} \\ u_z &= -k_{21}e_2 - k_{22}|e_2|^{\lambda_2} sign(e_2) - \bar{\bar{f}}_2 \\ &\quad - \frac{\varepsilon_{23}}{2} e_2 \hat{\theta}_{21} S_2^T(Z_2) S_2(Z_2) - \hat{\theta}_{22}\tanh\left(\frac{e_2}{b_2}\right) \end{aligned} \tag{27}$$

where q_c is the virtual control law, and u_z is the control input. k_{11}, k_{12}, ε_{11}, ε_{13}, b_1, k_{21}, k_{22} and ε_{23} are positive design constants. $0 < \lambda_2 < 1$. $\hat{\theta}_{11}$, $\hat{\theta}_{12}$ are the estimations of θ_{11}, θ_{12}, respectively. $\hat{\theta}_{21}$, $\hat{\theta}_{22}$ are the estimations of θ_{21}, θ_{22}, respectively. $\theta_{11}, \theta_{12}, \theta_{21}, \theta_{22}$ are unknown constants and will be specified later. $\bar{f}_1$ and $\bar{\bar{f}}_2$ are known functions and will be specified in (42) and (52). $Z_1 = \left[\alpha, e_u, e_l, \varpi_1, \hat{\theta}_{12}\right]^T$, $Z_2 = \left[\alpha, q, e_u, e_l, \varpi_1, e_2, \hat{\theta}_{11}, \hat{\theta}_{12}\right]^T$. And $\psi_{11}(\varpi_1)$ is a continuous but not smooth function, which is given by

$$\psi_{11}(\varpi_1) = \begin{cases} |\varpi_1|^{\lambda_1} sign(\varpi_1), & |\varpi_1| > \varepsilon_{\varpi 1} \\ \varepsilon_{\varpi 1}^{\lambda_1 - 1}\varpi_1, & |\varpi_1| \leq \varepsilon_{\varpi 1} \end{cases} \tag{28}$$

where $\varepsilon_{\varpi 1} > 0$ is a designed constant. $0 < \lambda_1 = \frac{p_1}{p_2} < 1$.

And the adaptive laws are designed as

$$\begin{aligned} \dot{\hat{\theta}}_{11} &= -k_{\theta 11}\hat{\theta}_{11} + \frac{k'_{\theta 11}\varepsilon_{13}}{2}\varpi_1^2 S_1^T(Z_1) S_F(Z_1) \\ \dot{\hat{\theta}}_{12} &= -k'_{\theta 12}\hat{\theta}_{12} + k_{\theta 12}\varpi_1 \tanh\left(\frac{\varpi_1}{b_1}\right) \\ \dot{\hat{\theta}}_{21} &= -k_{\theta 21}\hat{\theta}_{21} + \frac{k'_{\theta 21}\varepsilon_{23}}{2} e_2^2 S_2^T(Z_2) S_2(Z_2) \\ \dot{\hat{\theta}}_{22} &= -k'_{\theta 22}\hat{\theta}_{22} + k_{\theta 22} e_2 \tanh\left(\frac{e_2}{b_2}\right) \end{aligned} \tag{29}$$

where $\theta_{11}(0) \geq 0, \theta_{12}(0) \geq 0, \theta_{21}(0) \geq 0, \theta_{22}(0) \geq 0, k_{\theta 11}$, $k'_{\theta 11}$, $k_{\theta 12}$, $k'_{\theta 12}$, $k_{\theta 21}$, $k_{\theta 22}$, $k'_{\theta 22}$, $k'_{\theta 21}$ are positive design constants. It is worth noting that $\hat{\theta}_{11}(t) \geq 0$, $\hat{\theta}_{12}(t) \geq 0$, $\hat{\theta}_{21}(t) \geq 0, \hat{\theta}_{22}(t) \geq 0$ can be guaranteed under non-negative initial values.

Remark 4: In the traditional finite-time control, the derivative of the virtual control law is singular at the origin. To avoid the singularity problem, the continuous function $\psi_{11}(\varpi_1)$ is introduced into the virtual control law q_c in (27). However, the derivative of this function is not continuous, which will bring a great challenge to the stability analysis. Hence, the common Lyapunov functional method and Lemma 7 will be combined to prove stability of the closed-loop system (26) and (27).

To deal with non-strict feedback terms $H_1(\alpha, q, t)$ and $H_2(\alpha, q, t)$, the following lemma is required:

Lemma 8: Defining $x = [\alpha, q]^T$, the following inequality is guaranteed:

$$\|x\| \leq \Phi\left(e_u, e_l, \varpi_1, \hat{\theta}_{11}, \hat{\theta}_{12}\right)|\varpi_1| + |e_2| + M_{\alpha c} \tag{30}$$

where $\Phi\left(e_u, e_l, \varpi_1, \hat{\theta}_{11}, \hat{\theta}_{12}\right)$ is given in (35). $M_{S1} > 0$ is a constant, and $S_1^T(Z_1) S_1(Z_1) \leq M_{S1}$. $M_{\alpha c} > 0$ and $M'_{\alpha c} > 0$ are known constants, and $|\alpha_c| < M'_{\alpha c}, M'_{\alpha c} + \left|\frac{1-Q}{2}\right| b(t) \leq M_{\alpha c}$. $\psi_{12}(\varpi_1)$ is a continuous function, which is given by

$$\psi_{12}(\varpi_1) = \begin{cases} |\varpi_1|^{\lambda_1 - 1}, & |\varpi_1| > \varepsilon_{\varpi 1} \\ \varepsilon_{\varpi 1}^{\lambda_1 - 1}, & |\varpi_1| \leq \varepsilon_{\varpi 1} \end{cases} \tag{31}$$

Proof: According to (21), we have

$$\begin{aligned} |e_1| &= \left|\frac{e_u - e_l}{\pi} \frac{\partial \arctan(\varpi_1)}{\partial \varpi_1}\right| |\varpi_1| + \left|\frac{e_u + e_l}{2}\right| \\ &\leq \left|\frac{e_u - e_l}{\pi}\right| |\varpi_1| + \left|\frac{e_u + e_l}{2}\right| \end{aligned} \tag{32}$$

Further, invoking (8) and Definition 1, (32) can be written as

$$|e_1| \leq \left|\frac{e_u - e_l}{\pi}\right| |\varpi_1| + \left|\frac{1-Q}{2}\right| b(t) \tag{33}$$

where $\left|\frac{1-Q}{2}\right| b(t)$ is bounded.

Considering (27), (33) and the fact that $S_1^T(Z_1) S_1(Z_1) \leq M_{S1}$, we obtain

$$\begin{aligned} \|x\| &\leq |\alpha| + |q| \leq |e_1| + |\alpha_c| + |e_2| + |q_c| \\ &= |e_1| + |\alpha_c| + |e_2| \\ &\quad + \left| g_1^{-1} \begin{pmatrix} k_{11}\varpi_1 + k_{12}\psi_{11}(\varpi_1) + \frac{\varepsilon_{11}}{2}\varpi_1 \bar{f}_1^2 \\ + \frac{\varepsilon_{11}}{2}\varpi_1 \hat{\theta}_{11} S_1^T(Z_1) S_1(Z_1) \\ + \hat{\theta}_{12} \tanh\left(\frac{\varpi_1}{b_1}\right) + \frac{1}{2}\varpi_1 g_1^2 \end{pmatrix} \right| \\ &\leq \left|\frac{e_u - e_l}{\pi}\right| |\varpi_1| + \left|\frac{1-Q}{2}\right| b(t) + M'_{\alpha c} + |e_2| \\ &\quad + g_1^{-1}\left(k_{11} + \frac{\varepsilon_{11}}{2}\bar{f}_1^2 + \frac{1}{2}g_1^2\right)|\varpi_1| + \frac{g_1^{-1}}{b_1}\hat{\theta}_{12}|\varpi_1| \\ &\quad + g_1^{-1} k_{12}\psi_{12}(\varpi_1)|\varpi_1| + g_1^{-1}\frac{\varepsilon_{11}}{2}\varpi_1 \hat{\theta}_{11} M_{S1}|\varpi_1| \\ &\leq \Phi\left(e_u, e_l, \varpi_1, \hat{\theta}_{11}, \hat{\theta}_{12}\right)|\varpi_1| + |e_2| + M_{\alpha c} \end{aligned} \tag{34}$$

where $M'_{\alpha c} + \left|\frac{1-Q}{2}\right| b(t) \leq M_{\alpha c}$, and

$$\begin{aligned} &\Phi\left(e_u, e_l, \varpi_1, \hat{\theta}_{11}, \hat{\theta}_{12}\right) \\ &= \left|\frac{e_u - e_l}{\pi\left(1 + \varpi_1^2\right)}\right| \\ &\quad + g_1^{-1}\left(k_{11} + \frac{\varepsilon_{11}}{2}\bar{f}_1^2 + \frac{1}{2}g_1^2\right) + g_1^{-1} k_{12}\psi_{12}(\varpi_1) \\ &\quad + g_1^{-1}\frac{\varepsilon_{11}}{2}\varpi_1 \hat{\theta}_{11} M_{S1} + \frac{g_1^{-1}}{b_1}\hat{\theta}_{12} \end{aligned} \tag{35}$$

This concludes the proof.◇

Next, a detailed stability analysis will be carried out for the closed-loop system (26), (27), (29), and the whole analysis process will be divided into the following three steps.

Step 1: The first subsystem of (26) can be written as

$$\dot{\varpi}_1 = g_1(f_1 + \Delta f_1 + q + H_1 - \dot{\alpha}_c) + N \tag{36}$$

For subsystem (36), we choose the following Lyapunov function:

$$V_1 = \frac{1}{2}\varpi_1^2 + \Omega_1 \tag{37}$$

where $\Omega_1 = \frac{e^{-\lambda_1(t-\bar{\tau}_1)}}{2(1-\dot{\bar{\tau}}_1^*)}\bar{\tau}_1 \int_{t-\tau_1(t)}^{t} \int_{\iota}^{t} e^{\lambda_1 s} h_1^2(\alpha(s), q(s))\, ds d\iota$; $\lambda_1 > 0$ is a design constant.

In (37), Ω_1 can be written as

$$\Omega_1 = \frac{e^{-\lambda_1(t-\bar{\tau}_1)}}{2\left(1 - \dot{\bar{\tau}}_1^*\right)}\bar{\tau}_1 \int_{t-\tau_1(t)}^{t} \hbar_1(\iota, t) d\iota \tag{38}$$

where $\hbar_1(\iota, t) = \int_{\iota}^{t} e^{\lambda_1 s} h_1^2(\alpha(s), q(s))\, ds$.

Then, the time derivative of Ω_1 can be obtained is given in (39), as shown at the bottom of the next page.

Invoking Assumption 1 and the fact $t - \tau_1 \leq s \leq t$, we have

$$\begin{aligned} \frac{(1 - \dot{\tau}_1)}{\left(1 - \dot{\bar{\tau}}_1^*\right)} &\geq 1 \\ e^{-\lambda_1(t - \bar{\tau}_1 - s)} &\geq e^{-\lambda_1(-\bar{\tau}_1 + \tau_1)} \geq 1 \end{aligned} \tag{40}$$

Then, substituting (40) into (39) yields

$$\dot{\Omega}_1 \leq -\lambda_1 \Omega_1 - \frac{1}{2}\bar{\tau}_1 H'_1 + \frac{\bar{\tau}_1^2 e^{\bar{\tau}_1}}{2\left(1 - \dot{\bar{\tau}}_1^*\right)} h_1^2(\alpha, q) \tag{41}$$

where $H'_1 = \int_{t-\tau_1(t)}^{t} h_1^2(\alpha(s), q(s))\, ds$.

Based on (36) and (41), the time derivative of V_1 is given by

$$\begin{aligned} \dot{V}_1 &= \varpi_1 \dot{\varpi}_1 + \dot{\Omega}_1 \\ &= \varpi_1 \begin{pmatrix} g_1 f_1(\alpha) + g_1 \Delta f_1(\alpha) + g_1 q \\ + g_1 H_1 - g_1 \dot{\alpha}_c + N \end{pmatrix} + \dot{\Omega}_1 \end{aligned}$$

$$\leq \varpi_1\left(\frac{\varepsilon_{11}}{2}\varpi_1\bar{f}_1^2+g_1\Delta f_1(\alpha)+g_1q+g_1H_1\right)-\lambda_1\Omega_1-\frac{1}{2}\bar{\tau}_1H'_1+\frac{\bar{\tau}_1^2e^{\bar{\tau}_1}}{2\left(1-\bar{\tau}_1^*\right)}h_1^2(\alpha,q)+\frac{1}{2\varepsilon_{11}} \tag{42}$$

where $\bar{f}_1=g_1f_1(\alpha)-g_1\dot{\alpha}_c+N(e_1,e_u,e_l)$.

Based on Lemma 4, we have

$$\begin{aligned}\varpi_1g_1H_1&=\varpi_1g_1\int_{t-\tau_1(t)}^{t}h_1(\alpha,q)\,ds\\&\leq\frac{1}{2}\varpi_1^2g_1^2+\frac{1}{2}\left(\int_{t-\tau_1(t)}^{t}h_1(\alpha(s),q(s))\,ds\right)^2\\&\leq\frac{1}{2}\varpi_1^2g_1^2+\frac{1}{2}\tau_1(t)\int_{t-\tau_1(t)}^{t}h_1^2(\alpha(s),q(s))\,ds\\&\leq\frac{1}{2}\varpi_1^2g_1^2+\frac{1}{2}\bar{\tau}_1H'_1\end{aligned} \tag{43}$$

Substituting (43) into (42) yields

$$\begin{aligned}\dot{V}_1&\leq\varpi_1\left(\frac{\varepsilon_{11}}{2}\varpi_1\bar{f}_1^2+g_1\Delta f_1(\alpha)+g_1q+\frac{1}{2}\varpi_1g_1^2\right)+\frac{1}{2}\bar{\tau}_1H_1{}'-\lambda_1\Omega_1-\frac{1}{2}\bar{\tau}_1H'_1+\frac{\bar{\tau}_1^2e^{\bar{\tau}_1}}{2\left(1-\bar{\tau}_1^*\right)}h_1^2(\alpha,q)+\frac{1}{2\varepsilon_{11}}\\&\leq\varpi_1\left(\frac{\varepsilon_{11}}{2}\varpi_1\bar{f}_1^2+g_1\Delta f_1(\alpha)+g_1q+\frac{1}{2}\varpi_1g_1^2\right)-\lambda_1\Omega_1+c_{13}N_1(\|x\|)+\frac{1}{2\varepsilon_{11}}\end{aligned} \tag{44}$$

where $c_{13}=\frac{\bar{\tau}_1^2e^{\bar{\tau}_1}}{2(1-\bar{\tau}_1^*)}$.

Step 2: The subsystem of (26) can be written as

$$\dot{q}=f_2+\Delta f_2+g_2u_z+\rho g'_2\zeta(u_z)+H_2 \tag{45}$$

Based on (27), the time derivative of q_c can be written as

$$\begin{aligned}\dot{q}_c=&\frac{\partial q_c}{\partial\alpha}(f_1(\alpha)+q)+\frac{\partial q_c}{\partial\alpha}H_1+\frac{\partial q_c}{\partial\alpha}\Delta f_1(\alpha)+\frac{\partial q_c}{\partial\dot{\alpha}_c}\ddot{\alpha}_c+\frac{\partial q_c}{\partial e_u}\dot{e}_u+\frac{\partial q_c}{\partial e_l}\dot{e}_l+\frac{\partial q_c}{\partial\hat{\theta}_{11}}\dot{\hat{\theta}}_{11}+\frac{\partial q_c}{\partial\hat{\theta}_{12}}\dot{\hat{\theta}}_{12}+\frac{\partial q_c}{\partial\alpha_c}\dot{\alpha}_c\\&+\frac{\partial q_c}{\partial\varpi_1}(g_1(f_1+\Delta f_1+q+H_1-\dot{\alpha}_c)+N)\\=&Q_{11}+Q_{12,\delta(t)}+Q_{13,\delta(t)}H_1\end{aligned} \tag{46}$$

where $Q_{11}=\frac{\partial q_c}{\partial\alpha}(f_1(\alpha)+q)+\frac{\partial q_c}{\partial\dot{\alpha}_c}\ddot{\alpha}_c+\frac{\partial q_c}{\partial e_u}\dot{e}_u+\frac{\partial q_c}{\partial e_l}\dot{e}_l+\frac{\partial q_c}{\partial\hat{\theta}_{11}}\dot{\hat{\theta}}_{11}+\frac{\partial q_c}{\partial\hat{\theta}_{12}}\dot{\hat{\theta}}_{12}+\frac{\partial q_c}{\partial\alpha_c}\dot{\alpha}_c$, $Q_{12,\delta(t)}=\frac{\partial q_c}{\partial\alpha}\Delta f_1(\alpha)+\frac{\partial q_c}{\partial\varpi_1}(g_1(f_1+\Delta f_1+q-\dot{\alpha}_c)+N)$, $Q_{13,\delta(t)}=\left(\frac{\partial q_c}{\partial\varpi_1}g_1+\frac{\partial q_c}{\partial\alpha}\right)$.

It should be noted that $\delta(t):[0,+\infty)\to\Lambda=\{1,2\}$ stands for a piecewise continuous switching signal, which is caused by the discontinuity of $\frac{\partial q_c}{\partial\varpi_1}$. Therefore, the derivative of q_c is divided into continuous part Q_{11}, discontinuous part $Q_{12,\delta(t)}$, and the part related to distributed delay term $Q_{13,\delta(t)}$. And these three parts will be dealt with separately in the following.

For subsystem (45), we choose the following Lyapunov function:

$$V_2=\frac{1}{2}e_2^2+\frac{1}{\sigma}\Omega_1+\frac{1}{\sigma}\Omega_2 \tag{47}$$

where $\Omega_2=\frac{e^{-\lambda_2(t-\bar{\tau}_2)}}{2(1-\bar{\tau}_2^*)}\bar{\tau}_2\int_{t-\tau_2(t)}^{t}\int_{\iota}^{t}e^{\lambda_2 s}h_2^2(\alpha(s),q(s))\,ds\,d\iota$. $\lambda_2>0$ is a design constant. And σ is an unknown constant, which is defined in (25).

Similar to (41), the time derivative of Ω_2 is given by

$$\dot{\Omega}_2\leq-\lambda_2\Omega_2-\frac{1}{2}\bar{\tau}_2H'_2+\frac{\bar{\tau}_2^2e^{\bar{\tau}_2}}{2\left(1-\bar{\tau}_2^*\right)}h_2^2(\alpha,q) \tag{48}$$

where $H'_2=\int_{t-\tau_2(t)}^{t}h_2^2(\alpha(s),q(s))\,ds$.

Invoking (26), (41), (46) and (48), the time derivative of V_2 is given by

$$\begin{aligned}\dot{V}_2&=e_2\dot{e}_2+\frac{1}{\sigma}\dot{\Omega}_1+\frac{1}{\sigma}\dot{\Omega}_2\\&=e_2\left(\begin{matrix}f_2(\alpha,q)+\Delta f_2(\alpha,q)+g_2u_z+\rho g'_2\zeta(u_z)\\+H_2-Q_{11}-Q_{12,\delta(t)}-Q_{13,\delta(t)}H_1\end{matrix}\right)+\frac{1}{\sigma}\dot{\Omega}_1+\frac{1}{\sigma}\dot{\Omega}_2\end{aligned} \tag{49}$$

Similar to (43), we have

$$\begin{aligned}-e_2Q_{13,\delta(t)}H_1&\leq\frac{\sigma}{2}e_2^2Q_{13,\delta(t)}^2+\frac{1}{2\sigma}\bar{\tau}_1H'_1\\e_2H_2&\leq\frac{\sigma}{2}e_2^2+\frac{1}{2\sigma}\bar{\tau}_2H'_2\end{aligned} \tag{50}$$

$$\dot{\Omega}_1=-\lambda_1\Omega_1+\frac{e^{-\lambda_1(t-\bar{\tau}_1)}}{2\left(1-\bar{\tau}_1^*\right)}\bar{\tau}_1\left(\hbar_1(t,t)-(1-\dot{\tau}_1)\hbar_1(t-\tau_1(t),t)+\int_{t-\tau_1(t)}^{t}\frac{\partial\hbar_1(\iota,t)}{\partial t}d\iota\right)$$
$$=-\lambda_1\Omega_1-\bar{\tau}_1\frac{(1-\dot{\tau}_1)}{2\left(1-\bar{\tau}_1^*\right)}\int_{t-\tau_1(t)}^{t}e^{-\lambda_1(t-\bar{\tau}_1-s)}h_1^2(\alpha(s),q(s))\,ds+\bar{\tau}_1\tau_1\frac{e^{\bar{\tau}_1}}{2\left(1-\bar{\tau}_1^*\right)}h_1^2(\alpha,q) \tag{39}$$

Substituting (50) into (49) yields

$$\begin{aligned}\dot{V}_2 \le\ & e_2\begin{pmatrix} f_2(\alpha,q)+\Delta f_2(\alpha,q)+g_2u_z+\rho g'_2\zeta\left(u_z\right) \\ -Q_{11}-Q_{12,\delta(t)}+\frac{\sigma}{2}e_2+\frac{\sigma}{2}e_2Q^2_{13,\delta(t)}\end{pmatrix} \\ &+\frac{1}{2\sigma}\bar{\tau}_2H'_2+\frac{1}{2\sigma}\bar{\tau}_1H'_1+\frac{1}{\sigma}\dot{\Omega}_1+\frac{1}{\sigma}\dot{\Omega}_2 \\ \le\ & e_2\begin{pmatrix} \frac{\varepsilon_{21}\sigma}{2}e_2\bar{f}_2^2+\Delta f_2+g_2u_z+\rho g'_2\zeta\left(u_z\right) \\ -Q_{12,\delta(t)}+\frac{\sigma}{2}e_2+\frac{\sigma}{2}e_2Q^2_{13,\delta(t)}\end{pmatrix} \\ &+\frac{1}{2\varepsilon_{21}\sigma}+\frac{1}{2\sigma}\bar{\tau}_2H'_2+\frac{1}{2\sigma}\bar{\tau}_1H'_1 \\ &+\frac{1}{\sigma}\left(-\lambda_1\Omega_1-\frac{1}{2}\bar{\tau}_1H'_1+\frac{\bar{\tau}_1^2e^{\bar{\tau}_1}}{2\left(1-\bar{\tau}_1^*\right)}h_1^2\left(\alpha,q\right)\right) \\ &+\frac{1}{\sigma}\left(-\lambda_2\Omega_2-\frac{1}{2}\bar{\tau}_2H'_2+\frac{\bar{\tau}_2^2e^{\bar{\tau}_2}}{2\left(1-\bar{\tau}_2^*\right)}h_2^2\left(\alpha,q\right)\right)\end{aligned} \tag{51}$$

where $\bar{f}_2=f_2(\alpha,q)-Q_{11}$.

Invoking Assumption 2, (51) can be written as

$$\begin{aligned}\dot{V}_2 \le\ & e_2\begin{pmatrix} \sigma\bar{\bar{f}}_2+\Delta f_2+g_2u_z+\rho g'_2\zeta\left(u_z\right) \\ -Q_{12,\delta(t)}+\frac{\sigma}{2}e_2Q^2_{13,\delta(t)}\end{pmatrix} \\ &+\frac{1}{2\varepsilon_{21}\sigma}-\frac{\lambda_1}{\sigma}\Omega_1-\frac{\lambda_2}{\sigma}\Omega_2 \\ &+\frac{c_{13}}{\sigma}N_1\left(\|x\|\right)+\frac{c_{23}}{\sigma}N_2\left(\|x\|\right)\end{aligned} \tag{52}$$

where $\bar{\bar{f}}_2=\frac{\varepsilon_{21}}{2}e_2\bar{f}_2^2+\frac{1}{2}e_2$, $c_{13}=\frac{\bar{\tau}_1^2e^{\bar{\tau}_1}}{2(1-\bar{\tau}_1^*)}$, $c_{23}=\frac{\bar{\tau}_2^2e^{\bar{\tau}_2}}{2(1-\bar{\tau}_2^*)}$.

Step 3: So far, Lyapunov functions have been designed for (36) and (45). Further, define $V'=V_1+V_2$. Then, the time derivative of V' is given by

$$\begin{aligned}\dot{V}'\ \le\ & \varpi_1\left(\frac{\varepsilon_{11}}{2}\varpi_1\bar{f}_1^2+g_1\Delta f_1(\alpha)+g_1q+\frac{1}{2}\varpi_1g_1^2\right) \\ &-\lambda_1\Omega_1+e_2\begin{pmatrix} \sigma\bar{\bar{f}}_2+\Delta f_2+g_2u_z+\rho g'_2\zeta\left(u_z\right) \\ -Q_{12,\delta(t)}+\frac{\sigma}{2}e_2Q^2_{13,\delta(t)}\end{pmatrix} \\ &-\frac{\lambda_1}{\sigma}\Omega_1-\frac{\lambda_2}{\sigma}\Omega_2+\left(\frac{c_{13}}{\sigma}+c_{13}\right)N_1\left(\|x\|\right) \\ &+\frac{c_{23}}{\sigma}N_2\left(\|x\|\right)+\frac{1}{2\tau_{11}}+\frac{1}{2\varepsilon_{21}\sigma}\end{aligned} \tag{53}$$

According to Lemma 8 and Remark 2, we have

$$\begin{aligned}N_1\left(\|x\|\right) &\le N_1\left(\Phi\left|\varpi_1\right|+\left|e_2\right|+M_{\alpha c}\right) \\ &\le N_1\left(3\Phi\left|\varpi_1\right|\right)+N_1\left(3\left|e_2\right|\right)+N_1\left(3M_{\alpha c}\right) \\ &\le 3\Phi\left|\varpi_1\right|\overline{N}_1\left(3\Phi\left|\varpi_1\right|\right)+3\left|e_2\right|\overline{N}_1\left(3\left|e_2\right|\right) \\ &\quad +N_1\left(3M_{\alpha c}\right) \\ &\le \frac{\varepsilon_{N1}}{2}9\Phi^2\bar{N}_1^2\left(3\Phi\left|\varpi_1\right|\right)\varpi_1^2+\frac{1}{\varepsilon_{N1}} \\ &\quad +\frac{\varepsilon_{N1}}{2}9\bar{N}_1^2\left(3\left|e_2\right|\right)e_2^2+N_1\left(3M_{\alpha c}\right)\end{aligned} \tag{54}$$

where $\varepsilon_{N1}>0$ is a design constant.

Similar to (54), the following can easily be obtained:

$$\begin{aligned}N_2\left(\|x\|\right) \le\ & \frac{\varepsilon_{N2}}{2}9\Phi^2\bar{N}_2^2\left(3\Phi\left|\varpi_1\right|\right)\varpi_1^2 \\ &+\frac{\varepsilon_{N2}}{2}9\bar{N}_2^2\left(3\left|e_2\right|\right)e_2^2+\frac{1}{\varepsilon_{N2}}+N_2\left(3M_{\alpha c}\right)\end{aligned} \tag{55}$$

where $\varepsilon_{N2}>0$ is a design constant.

Based on (54) and (55), we have

$$\begin{aligned}&\frac{c_{13}+\sigma c_{13}}{\sigma}N_1\left(\|x\|\right)+\frac{c_{23}}{\sigma}N_2\left(\|x\|\right) \\ &\le \frac{c_{13}+\sigma c_{13}}{\sigma}\begin{pmatrix} \frac{\varepsilon_{N1}}{2}9\Phi^2\overline{N}_1^2\left(3\Phi\left|\varpi_1\right|\right)\varpi_1^2+\frac{1}{\varepsilon_{N1}} \\ +\frac{\varepsilon_{N1}}{2}9\overline{N}_1^2\left(3\left|e_2\right|\right)e_2^2+N_1\left(3M_{\alpha c}\right)\end{pmatrix} \\ &\quad +\frac{c_{23}}{\sigma}\begin{pmatrix} \frac{\varepsilon_{N2}}{2}9\Phi^2\overline{N}_2^2\left(3\Phi\left|\varpi_1\right|\right)\varpi_1^2+\frac{1}{\varepsilon_{N2}} \\ +\frac{\varepsilon_{N2}}{2}9\overline{N}_2^2\left(3\left|e_2\right|\right)e_2^2+N_2\left(3M_{\alpha c}\right)\end{pmatrix} \\ &= \bar{\bar{N}}_{\varpi 1}\varpi_1^2+\bar{\bar{N}}_{e2}e_2^2+C_N\end{aligned} \tag{56}$$

where $\bar{\bar{N}}_{\varpi 1}=\left(\frac{c_{13}}{\sigma}+c_{13}\right)\frac{\varepsilon_{N1}}{2}9\Phi^2\overline{N}_1^2\left(3\Phi\left|\varpi_1\right|\right)+\frac{c_{23}}{\sigma}\frac{\varepsilon_{N2}}{2}9\Phi^2\overline{N}_2^2\left(3\Phi\left|\varpi_1\right|\right)$, $\bar{\bar{N}}_{e2}=\left(\frac{c_{13}}{\sigma}+c_{13}\right)\frac{\varepsilon_{N1}}{2}9\overline{N}_1^2\left(3\left|e_2\right|\right)+\frac{c_{23}}{\sigma}\frac{\varepsilon_{N2}}{2}9\overline{N}_2^2\left(3\left|e_2\right|\right)+\varpi_1g_1$, $C_N=\left(\frac{c_{13}}{\sigma}+c_{13}\right)N_1\left(3M_{\alpha c}\right)+\frac{c_{23}}{\sigma}N_2\left(3M_{\alpha c}\right)+\left(\frac{c_{13}}{\sigma}+c_{13}\right)\frac{1}{\varepsilon_{N1}}+\frac{c_{23}}{\sigma}\frac{1}{\varepsilon_{N2}}$.

Substituting (56) into (53) yields

$$\begin{aligned}\dot{V}'\ \le\ & \varpi_1\left(\frac{\varepsilon_{11}}{2}\varpi_1\bar{f}_1^2+\Delta\bar{f}_1+g_1q_c+\frac{1}{2}\varpi_1g_1^2\right)-\lambda_1\Omega_1 \\ &+e_2\left(\sigma\bar{\bar{f}}_2+\Delta\bar{f}_{2,\delta(t)}+g_2u_z+\rho g'_2\zeta\left(u_z\right)\right) \\ &-\frac{\lambda_1}{\sigma}\Omega_1-\frac{\lambda_2}{\sigma}\Omega_2+C'_N\end{aligned} \tag{57}$$

where $\Delta\bar{f}_1=g_1\Delta f_1(\alpha)+\bar{\bar{N}}_{\varpi 1}\varpi_1$, $\Delta\bar{f}_{2,\delta(t)}=\Delta f_2+\bar{\bar{N}}_{e2}e_2-Q_{12,\delta(t)}+\frac{\sigma}{2}e_2Q^2_{13,\delta(t)}$, $C'_N=C_N+\frac{1}{2\tau_{11}}+\frac{1}{2\varepsilon_{21}\sigma}$.

According to Lemma1, there exist unknown RBFNNs, which can approximate the unknown functions $\Delta\bar{f}_1$ and $\Delta\bar{f}_{2,\delta(t)}$, such that for any given constants $M_{NN1}>0$ and $M_{NN2}>0$ we have

$$\begin{aligned}\Delta\bar{f}_1 &= {W_1^*}^TS_1\left(Z'_1\right)+\bar{\varepsilon}^*_{NN1}\left(Z'_1\right) \\ \Delta\bar{f}_{2,\delta(t)} &= {W_{2,\delta(t)}}^{*T}S_2\left(Z_2\right)+\bar{\varepsilon}^*_{NN2,\delta(t)}\left(Z_2\right)\end{aligned} \tag{58}$$

where $\left|\bar{\varepsilon}^*_{NN1}\left(Z'_1\right)\right|\le M_{NN1}$, $\left|\bar{\varepsilon}^*_{NN2,\delta(t)}\left(Z_2\right)\right|\le M_{NN2}$, and $Z'_1=\left[\alpha,e_u,e_l,\varpi_1,\hat{\theta}_{11},\hat{\theta}_{12}\right]^T$.

Based on (58), we have

$$\begin{aligned}\varpi_1\Delta\bar{f}_1 &= \varpi_1{W_1^*}^TS_1\left(Z'_1\right)+\varpi_1\bar{\varepsilon}^*_{NN1}\left(Z'_1\right) \\ &\le \frac{\varepsilon_{13}}{2}\varpi_1^2\left\|W_1^*\right\|^2S_1^T\left(Z'_1\right)S_1\left(Z'_1\right) \\ &\quad +\frac{1}{2\varepsilon_{13}}+\left|\varpi_1\right|\theta_{12} \\ &\le \frac{\varepsilon_{13}}{2}\varpi_1^2\theta_{11}S_1^T\left(Z'_1\right)S_1\left(Z'_1\right) \\ &\quad +\frac{1}{2\varepsilon_{13}}+\left|\varpi_1\right|\theta_{12}\end{aligned} \tag{59}$$

where $\|W_1^*\|^2\le\theta_{11}$, $\left|\bar{\varepsilon}^*_{NN1}\left(Z_1\right)\right|\le M_{NN2}<\theta_{12}$, $\theta_{12}>0$ is an unknown constant.

Invoking Lemma 2, (59) can be written as

$$\varpi_1 \Delta\bar{f}_1 \le \frac{\varepsilon_{13}}{2}\varpi_1^2\theta_{11}S_1^T(Z_1)S_1(Z_1)+\frac{1}{2\varepsilon_{13}}+|\varpi_1|\theta_{12} \quad (60)$$

Similar to (59), we have

$$\begin{aligned} & e_2\left(\Delta\bar{f}_{2,\delta(t)}+\rho g'_2\zeta(u_z)\right) \\ &= e_2\left({W_{2,\delta(t)}}^{*T}S_2(Z_2)+\bar{\varepsilon}^*_{NN2,\delta(t)}(Z_2)+\rho g'_2\zeta(u_z)\right) \\ &\le \frac{\varepsilon_{23}}{2}e_2^2\left\|{W_{2,\delta(t)}}^*\right\|^2 S_2^T(Z_2)S_2(Z_2)+\frac{1}{2\varepsilon_{23}} \\ &\quad + |e_2|\left|\bar{\varepsilon}^*_{NN2,\delta(t)}(Z_2)+\rho g'_2\zeta(u_z)\right| \\ &\le \frac{\sigma\varepsilon_{23}}{2}e_2^2\theta_{21}S_2^T(Z_2)S_2(Z_2)+\frac{1}{2\varepsilon_{23}}+\sigma|e_2|\theta_{22} \end{aligned} \quad (61)$$

where $\frac{\|{W_{2,\delta(t)}}^*\|^2}{\sigma} \le \theta_{21}$, $\frac{\left|\bar{\varepsilon}^*_{NN2,\delta(t)}(Z_2)+\rho g'_2\zeta(u_z)\right|}{\sigma} \le \theta_{22}$.

Substituting (60) and (61) into (57) yields

$$\begin{aligned} \dot{V}' \le{}& \varpi_1\left(\frac{\varepsilon_{11}}{2}\varpi_1\bar{f}_1^2+g_1q_c+\frac{1}{2}\varpi_1 g_1^2\right)+\frac{1}{2\varepsilon_{13}}+\frac{1}{2\varepsilon_{23}} \\ &+\frac{\varepsilon_{13}}{2}\varpi_1^2\theta_{11}S_1^T(Z_1)S_1(Z_1)+|\varpi_1|\theta_{12}-\lambda_1\Omega_1 \\ &+e_2\left(\sigma\bar{\bar{f}}_2+g_2u_z\right)+\frac{\sigma\varepsilon_{23}}{2}e_2^2\theta_{21}S_2^T(Z_2)S_2(Z_2) \\ &+\sigma|e_2|\theta_{22}-\frac{\lambda_1}{\sigma}\Omega_1-\frac{\lambda_2}{\sigma}\Omega_2+C'_N \end{aligned} \quad (62)$$

Considering that $\theta_{11}(t) \ge 0, \theta_{12}(t) \ge 0, \theta_{21}(t) \ge 0, \theta_{22}(t) \ge 0$, and $\bar{\bar{f}}_2$ is an odd function of e_2, we have that

$$\begin{aligned} & e_2g_2u_{z,\delta(t)} \\ &= -e_2g_2k_{21}e_2-e_2g_2k_{22}|e_2|^{\lambda_2}sign(e_2)-e_2g_2\bar{\bar{f}}_2 \\ &\quad -e_2g_2\frac{\varepsilon_{23}}{2}e_2\hat{\theta}_{21}S_2^T(Z_2)S_2(Z_2)-e_2g_2\hat{\theta}_{22}\tanh\left(\frac{e_2}{b_2}\right) \\ &\le -e_2\sigma k_{21}e_2-e_2\sigma k_{22}|e_2|^{\lambda_2}sign(e_2)-e_2\sigma\bar{\bar{f}}_2 \\ &\quad -e_2\sigma\frac{\varepsilon_{23}}{2}e_2\hat{\theta}_{21}S_2^T(Z_2)S_2(Z_2)-e_2\sigma\hat{\theta}_{22}\tanh\left(\frac{e_2}{b_2}\right) \end{aligned} \quad (63)$$

Substituting (27) and (63) into (62) yields

$$\begin{aligned} \dot{V}' \le{}& -k_{11}\varpi_1^2-k_{12}\varpi_1\psi_{11}(\varpi_1) \\ &-\frac{\varepsilon_{13}}{2}\varpi_1^2\tilde{\theta}_{11}S_1^T(Z_1)S_1(Z_1) \\ &+|\varpi_1|\theta_{12}-\varpi_1\hat{\theta}_{12}\tanh\left(\frac{\varpi_1}{b_1}\right)-\left(\lambda_1+\frac{\lambda_1}{\sigma}\right)\Omega_1 \\ &-\sigma k_{21}e_2^2-\sigma k_{22}|e_2|^{\lambda_2+1}-\frac{\sigma\varepsilon_{23}}{2}e_2^2\tilde{\theta}_{21}S_2^T(Z_2)S_2(Z_2) \\ &-e_2\sigma\hat{\theta}_{22}\tanh\left(\frac{e_2}{b_2}\right)+\sigma|e_2|\theta_{22}-\frac{\lambda_2}{\sigma}\Omega_2 \\ &+C'_N+\frac{1}{2\varepsilon_{13}}+\frac{1}{2\varepsilon_{23}} \end{aligned} \quad (64)$$

where $\tilde{\theta}_{11}=\hat{\theta}_{11}-\theta_{11}, \tilde{\theta}_{21}=\hat{\theta}_{21}-\theta_{21}$.

Finally, we choose the following Lyapunov function:

$$V = V'+\frac{1}{2k'_{\theta 11}}\tilde{\theta}_{11}^2+\frac{1}{2k_{\theta 12}}\tilde{\theta}_{12}^2+\frac{\sigma}{2k'_{\theta 21}}\tilde{\theta}_{21}^2+\frac{\sigma}{2k_{\theta 22}}\tilde{\theta}_{22}^2 \quad (65)$$

where $\tilde{\theta}_{12}=\hat{\theta}_{12}-\theta_{12}, \tilde{\theta}_{22}=\hat{\theta}_{22}-\theta_{22}$.

According to (64), the time derivative of V is given by

$$\begin{aligned} \dot{V} \le{}& -k_{11}\varpi_1^2-k_{12}\varpi_1\psi_{11}(\varpi_1)+|\varpi_1|\theta_{12} \\ &-\varpi_1\theta_{12}\tanh\left(\frac{\varpi_1}{b_1}\right)-\left(\lambda_1+\frac{\lambda_1}{\sigma}\right)\Omega_1 \\ &-\sigma k_{21}e_2^2-\sigma k_{22}|e_2|^{\lambda_2+1}-e_2\sigma\theta_{22}\tanh\left(\frac{e_2}{b_2}\right) \\ &+\sigma|e_2|\theta_{22}-\frac{\lambda_2}{\sigma}\Omega_2+C'_N+\frac{1}{2\varepsilon_{13}}+\frac{1}{2\varepsilon_{23}} \\ &-\frac{k_{\theta 11}}{k'_{\theta 11}}\tilde{\theta}_{11}\hat{\theta}_{11}-\frac{k'_{\theta 12}}{k_{\theta 12}}\tilde{\theta}_{12}\hat{\theta}_{12} \\ &-\frac{k_{\theta 21}\sigma}{k'_{\theta 21}}\tilde{\theta}_{21}\hat{\theta}_{21}-\frac{k'_{\theta 22}\sigma}{k_{\theta 22}}\tilde{\theta}_{22}\hat{\theta}_{22} \end{aligned} \quad (66)$$

According to Lemma 3, we have

$$\begin{aligned} |\varpi_1|\theta_{12}-\varpi_1\theta_{12}\tanh\left(\frac{\varpi_1}{b_1}\right) &\le b_1\theta_{12}\xi \\ \sigma|e_2|\theta_{22}-e_2\sigma\theta_{22}\tanh\left(\frac{e_2}{b_2}\right) &\le \sigma b_2\theta_{22}\xi \end{aligned} \quad (67)$$

Substituting (67) into (66) yields

$$\begin{aligned} \dot{V} \le{}& -k_{11}\varpi_1^2-k_{12}\varpi_1\psi_{11}(\varpi_1)+b_1\theta_{12}\xi \\ &-\left(\lambda_1+\frac{\lambda_1}{\sigma}\right)\Omega_1-\sigma k_{21}e_2^2-\sigma k_{22}|e_2|^{\lambda_2+1} \\ &+\sigma b_2\theta_{22}\xi-\frac{\lambda_2}{\sigma}\Omega_2+C'_N+\frac{1}{2\varepsilon_{13}}+\frac{1}{2\varepsilon_{23}} \\ &-\frac{k_{\theta 11}}{2k'_{\theta 11}}\tilde{\theta}_{11}^2+\frac{k_{\theta 11}}{2k'_{\theta 11}}\theta_{11}^2-\frac{k'_{\theta 12}}{2k_{\theta 12}}\tilde{\theta}_{12}^2+\frac{k'_{\theta 12}}{2k_{\theta 12}}\theta_{12}^2 \\ &-\frac{k_{\theta 21}\sigma}{2k'_{\theta 21}}\tilde{\theta}_{21}^2+\frac{k_{\theta 21}\sigma}{2k'_{\theta 21}}\theta_{21}^2-\frac{k'_{\theta 22}\sigma}{2k_{\theta 22}}\tilde{\theta}_{22}^2+\frac{k'_{\theta 22}\sigma}{2k_{\theta 22}}\theta_{22}^2 \\ \le{}& -k_{11}\varpi_1^2-k_{12}\varpi_1\psi_{11}(\varpi_1)-\left(\lambda_1+\frac{\lambda_1}{\sigma}\right)\Omega_1 \\ &-\sigma k_{21}e_2^2-\sigma k_{22}|e_2|^{\lambda_2+1}-\frac{\lambda_2}{\sigma}\Omega_2-\frac{k_{\theta 11}}{2k'_{\theta 11}}\tilde{\theta}_{11}^2 \\ &-\frac{k'_{\theta 12}}{2k_{\theta 12}}\tilde{\theta}_{12}^2-\frac{k_{\theta 21}\sigma}{2k'_{\theta 21}}\tilde{\theta}_{21}^2-\frac{k'_{\theta 22}\sigma}{2k_{\theta 22}}\tilde{\theta}_{22}^2+C''_N \end{aligned} \quad (68)$$

where $C''_N = C'_N+b_1\theta_{12}\xi+\sigma b_2\theta_{22}\xi+\frac{1}{2\varepsilon_{13}}+\frac{1}{2\varepsilon_{23}}+\frac{k_{\theta 11}}{2k'_{\theta 11}}\theta_{11}^2+\frac{k'_{\theta 12}}{2k_{\theta 12}}\theta_{12}^2+\frac{k_{\theta 21}\sigma}{2k'_{\theta 21}}\theta_{21}^2+\frac{k'_{\theta 22}\sigma}{2k_{\theta 22}}\theta_{22}^2$.

Theorem 1: Considering the longitudinal attitude motion model (1) in the presence of system uncertainties, unsteady disturbances, and input saturation, the controller is given by (27), and the adaptive laws are proposed as (29). If the parameters are selected properly, the desired signal can be tracked within a small bounded error, and other signals in the closed-loop system are bounded.

Proof: According to (29), the value of function $\psi_{11}(\varpi_1)$ depends on ϖ_1. Hence, in the stability analysis, we need to discuss the value of variable ϖ_1 in two cases.

Case 1: When $|\varpi_1| > \varepsilon_{\varpi 1}$, we have that $\psi_{11}(\varpi_1) = |\varpi_1|^{\lambda_1} sign(\varpi_1)$. Then, based on (68), the time derivative of V can be written as

$$\begin{aligned}\dot{V} \le & -k_{11}\varpi_1^2 - k_{12}|\varpi_1|^{\lambda_1+1} - \left(\lambda_1 + \frac{\lambda_1}{\sigma}\right)\Omega_1 \\ & - \sigma k_{21}e_2^2 - \sigma k_{22}|e_2|^{\lambda_2+1} - \frac{\lambda_2}{\sigma}\Omega_2 - \frac{k_{\theta 11}}{2k'_{\theta 11}}\tilde{\theta}_{11}^2 \\ & - \frac{k'_{\theta 12}}{2k_{\theta 12}}\tilde{\theta}_{12}^2 - \frac{k_{\theta 21}\sigma}{2k'_{\theta 21}}\tilde{\theta}_{21}^2 - \frac{k'_{\theta 22}\sigma}{2k_{\theta 22}}\tilde{\theta}_{22}^2 + C''_N \end{aligned} \tag{69}$$

Substituting $x_1 = \tilde{\theta}_{ij}^2$, $x_2 = 1$, $c_1 = \lambda_{ij}$, $c_2 = 1 - \lambda_{ij}$ and $c_3 = \lambda_{ij}^{-1}$ into Lemma 6 yields

$$\left(\tilde{\theta}_{ij}^2\right)^{\lambda_{ij}} \le \tilde{\theta}_{ij}^2 + \left(1 - \lambda_{ij}\right)\lambda_{ij}^{\frac{\lambda_{ij}}{1-\lambda_{ij}}} \tag{70}$$

where $0 < \lambda_{ij} < 1$ is a design constant, $i = 1, 2, j = 1, 2$.

Similar to (70), we have

$$\begin{aligned}\Omega_1^{\lambda_{\Omega 1}} &\le \Omega_1 + (1 - \lambda_{\Omega 1})\lambda_{\Omega_1}^{\frac{\lambda_{\Omega 1}}{1-\lambda_{\Omega 1}}} \\ \Omega_2^{\lambda_{\Omega 2}} &\le \Omega_2 + (1 - \lambda_{\Omega 2})\lambda_{\Omega 2}^{\frac{\lambda_{\Omega 2}}{1-\lambda_{\Omega 2}}}\end{aligned} \tag{71}$$

where $0 < \lambda_{\Omega 1} < 1$, $0 < \lambda_{\Omega 2} < 1$.

Based on (70) and (71), (69) can be written as

$$\begin{aligned}\dot{V} \le & -k_{11}\varpi_1^2 - k_{12}|\varpi_1|^{\lambda_1+1} - \left(\lambda_1 + \frac{\lambda_1}{\sigma}\right)\Omega_1^{\lambda_{\Omega 1}} \\ & - \sigma k_{21}e_2^2 - \sigma k_{22}|e_2|^{\lambda_2+1} - \frac{\lambda_2}{\sigma}\Omega_2^{\lambda_{\Omega 2}} \\ & - \frac{k_{\theta 11}}{2k'_{\theta 11}}\left(\tilde{\theta}_{11}^2\right)^{\lambda_{11}} - \frac{k'_{\theta 12}}{2k_{\theta 12}}\left(\tilde{\theta}_{12}^2\right)^{\lambda_{12}} \\ & - \frac{k_{\theta 21}\sigma}{2k'_{\theta 21}}\left(\tilde{\theta}_{21}^2\right)^{\lambda_{21}} - \frac{k'_{\theta 22}\sigma}{2k_{\theta 22}}\left(\tilde{\theta}_{22}^2\right)^{\lambda_{22}} + C_1 \end{aligned} \tag{72}$$

where $C_1 = C''_N + \left(\lambda_1 + \frac{\lambda_1}{\sigma}\right)(1 - \lambda_{\Omega 1})\lambda_{\Omega_1}^{\frac{\lambda_{\Omega 1}}{1-\lambda_{\Omega 1}}} + \frac{\lambda_2}{\sigma}(1 - \lambda_{\Omega 2})\lambda_{\Omega 2}^{\frac{\lambda_{\Omega 2}}{1-\lambda_{\Omega 2}}} + \frac{k_{\theta 11}}{2k'_{\theta 11}}(1 - \lambda_{11})\lambda_{11}^{\frac{\lambda_{11}}{1-\lambda_{11}}} + \frac{k'_{\theta 12}}{2k_{\theta 12}}(1 - \lambda_{12})\lambda_{12}^{\frac{\lambda_{12}}{1-\lambda_{12}}} + \frac{k_{\theta 21}\sigma}{2k'_{\theta 21}}(1 - \lambda_{21})\lambda_{21}^{\frac{\lambda_{21}}{1-\lambda_{21}}} + \frac{k'_{\theta 22}\sigma}{2k_{\theta 22}}(1 - \lambda_{22})\lambda_{22}^{\frac{\lambda_{22}}{1-\lambda_{22}}}$.

If we choose appropriate parameter values, the following equation is established:

$$\frac{\lambda_1 + 1}{2} = \lambda_{\Omega 1} = \frac{\lambda_2 + 1}{2} = \lambda_{\Omega 2} = \lambda_{11} = \lambda_{12} = \lambda_{21} = \lambda_{22} \tag{73}$$

Then, (72) can be written as

$$\begin{aligned}\dot{V} \le & -k_{12}2^{\frac{\lambda_1+1}{2}}\left(\frac{1}{2}\varpi_1^2\right)^{\frac{\lambda_1+1}{2}} - \lambda_1\Omega_1^{\lambda_{\Omega 1}} \\ & - \sigma k_{22}2^{\frac{\lambda_2+1}{2}}\left(\frac{1}{2}e_2^2\right)^{\frac{\lambda_2+1}{2}} - \lambda_1\sigma^{\lambda_{\Omega 1}-1}\left(\frac{1}{\sigma}\Omega_1\right)^{\lambda_{\Omega 1}} \\ & - \lambda_2\sigma^{\lambda_{\Omega 2}-1}\left(\frac{1}{\sigma}\Omega_2\right)^{\lambda_{\Omega 2}} \\ & - k_{\theta 11}\left(2k'_{\theta 11}\right)^{\lambda_{11}-1}\left(\frac{1}{2k'_{\theta 11}}\tilde{\theta}_{11}^2\right)^{\lambda_{11}} \\ & - k'_{\theta 12}(2k_{\theta 12})^{\lambda_{12}-1}\left(\frac{1}{2k_{\theta 12}}\tilde{\theta}_{12}^2\right)^{\lambda_{12}} \\ & - k_{\theta 21}\left(\frac{\sigma}{2k'_{\theta 21}}\right)^{1-\lambda_{21}}\left(\frac{\sigma}{2k'_{\theta 21}}\tilde{\theta}_{21}^2\right)^{\lambda_{21}} \\ & - k'_{\theta 22}\left(\frac{\sigma}{2k_{\theta 22}}\right)^{1-\lambda_{22}}\left(\frac{\sigma}{2k_{\theta 22}}\tilde{\theta}_{22}^2\right)^{\lambda_{22}} + C_1 \\ \le & -K_1V^{\frac{\lambda_1+1}{2}} + C_1 \end{aligned} \tag{74}$$

where $K_1 = min\{k_{12}2^{\frac{\lambda_1+1}{2}}, \lambda_1, \sigma k_{22}2^{\frac{\lambda_2+1}{2}}, k_{\theta 11}\left(2k'_{\theta 11}\right)^{\lambda_{11}-1}, k'_{\theta 12}(2k_{\theta 12})^{\lambda_{12}-1}, k_{\theta 21}\left(\frac{\sigma}{2k'_{\theta 21}}\right)^{1-\lambda_{21}}, k'_{\theta 22}\left(\frac{\sigma}{2k_{\theta 22}}\right)^{1-\lambda_{22}}, \lambda_1\sigma^{\lambda_{\Omega 1}-1}, \lambda_2\sigma^{\lambda_{\Omega 2}-1}\}$.

Then, according to Lemma 6, the nonlinear closed-loop system (1), (27) and (29) is SGPFS. And it is obvious that the transformed error ϖ_1 is bounded. Then, according to (21), it can be concluded that the tracking error e_1 satisfies $e_l < e_1 < e_u$. When $V > 1$, increasing the value of λ_1 can improve the convergence rate of the Lyapunov function V. When $V \le 1$, reducing the value of λ_1 can improve the convergence rate of the Lyapunov function V. Therefore, the selection of should be considered comprehensively.

Case 2: When $|\varpi_1| \le \varepsilon_{\varpi 1}$, we have $\psi_{11}(\varpi_1) = \varepsilon_{\varpi 1}^{\lambda_1-1}\varpi_1$. Then, based on (68), the time derivative of V can be written as

$$\begin{aligned}\dot{V} \le & -k_{11}\varpi_1^2 - k_{12}\varepsilon_{\varpi 1}^{\lambda_1-1}\varpi_1^2 - \left(\lambda_1 + \frac{\lambda_1}{\sigma}\right)\Omega_1 - \sigma k_{21}e_2^2 \\ & - \sigma k_{22}|e_2|^{\lambda_2+1} - \frac{\lambda_2}{\sigma}\Omega_2 - \frac{k_{\theta 11}}{2k'_{\theta 11}}\tilde{\theta}_{11}^2 - \frac{k'_{\theta 12}}{2k_{\theta 12}}\tilde{\theta}_{12}^2 \\ & - \frac{k_{\theta 21}\sigma}{2k'_{\theta 21}}\tilde{\theta}_{21}^2 - \frac{k'_{\theta 22}\sigma}{2k_{\theta 22}}\tilde{\theta}_{22}^2 + C''_N \\ \le & -2k_{11}\frac{1}{2}\varpi_1^2 - \lambda_1\Omega_1 - 2\sigma k_{21}\frac{1}{2}e_2^2 - \lambda_1\frac{1}{\sigma}\Omega_1 \\ & - \lambda_2\frac{1}{\sigma}\Omega_2 - k_{\theta 11}\frac{1}{2k'_{\theta 11}}\tilde{\theta}_{11}^2 - k'_{\theta 12}\frac{1}{2k_{\theta 12}}\tilde{\theta}_{12}^2 \\ & - k_{\theta 21}\frac{\sigma}{2k'_{\theta 21}}\tilde{\theta}_{21}^2 - k'_{\theta 22}\frac{\sigma}{2k_{\theta 22}}\tilde{\theta}_{22}^2 + C''_N \\ \le & -K_2V + C''_N \end{aligned} \tag{75}$$

where $K_2 = \min\left\{2k_{11}, \lambda_1, 2\sigma k_{21}, \lambda_1, \lambda_2, k_{\theta 11}, k'_{\theta 12}, k_{\theta 21}, k'_{\theta 22}\right\}$.

According to Lemma 5, the transformed error ϖ_1 is bounded. Similarly, we have that the tracking error e_1 satisfies $e_l < e_1 < e_u$.

In summary, the whole state space is divided into two parts: $\Xi_1 = \{X \,|\, |\varpi_1| \le \varepsilon_{\varpi 1}\}$ and $\Xi_2 = \{X \,|\, |\varpi_1| > \varepsilon_{\varpi 1}\}$, $X = [\alpha, q]^T$. When $X \in \Xi_2$, the closed-loop system (1), (27) and (29) is semiglobal practical finite-time stable. Once the error signal ϖ_1 converges to the origin ($X \in \Xi_1$), the structure of the controller (27), (29) will switch, and the closed-loop system (1), (27) and (29) will satisfy Lemma 5. The common

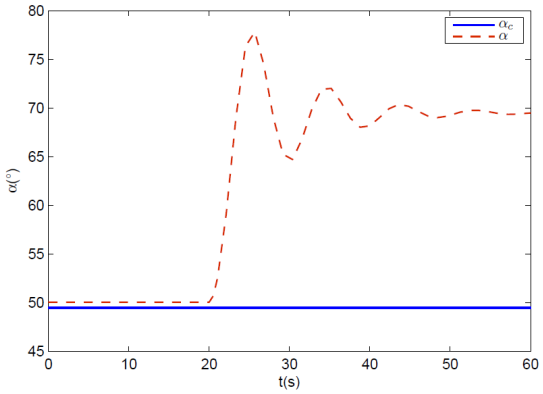

FIGURE 7. Tracking result of α ($\rho = 0.4$).

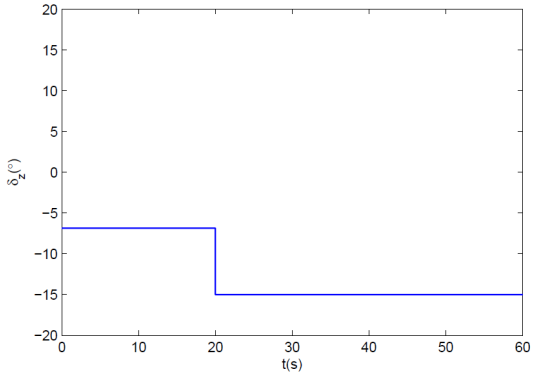

FIGURE 8. Control input signal ($\rho = 0.4$).

Lyapunov function (65) is designed to guarantee that the closed-loop system (1), (27) and (29) is stable under arbitrary switching. Hence, in the whole state space, the proposed controller can guarantee all signals bounded, especially the error signal ϖ_1. Then, according to (21), it can be concluded that the tracking error e_1 satisfies $e_l < e_1 < e_u$ in the whole state space.

V. SIMULATION STUDY

The aircraft model [8] and the unsteady disturbances $H_1(\alpha, q, t)$ and $H_2(\alpha, q, t)$ in (76) are used to verify the validity of the above designed controller (27).

$$C_{L,unsteady} = \int_{t-\tau_1(t)}^{t} e^{-b_L(\alpha(s))t} a_L(\alpha(s))\, q(s)\, ds$$
$$C_{m,unsteady} = \int_{t-\tau_2(t)}^{t} e^{-b_m(\alpha(s))t} a_m(\alpha(s))\, q(s)\, ds \quad (76)$$

where $b_L(\alpha)$, $a_L(\alpha)$, $b_m(\alpha)$, $a_m(\alpha)$ are continuous bounded functions of α, which can be easily obtained in [49].

A. DEEP STALL SIMULATION

To verify the results of the closed-loop bifurcation analysis, we perform closed-loop simulation of the system (1) and (12). We take the bifurcation analysis result in Fig. 4 as an example, and the control efficiency of the aircraft will be reduced in twentieth seconds ($\rho = 0.4$). The initial state of the aircraft is set as $\alpha = 50.0364^\circ$, $q = 0^\circ/s$, $T = 51815\ N$, and $\rho = 1$. The simulation results are given in Fig. 7 and Fig. 8.

In Fig. 7, α denotes the AOA response of the aircraft, and α_c is the AOA command. Fig. 7 shows that the aircraft can track the AOA before the control efficiency is reduced ($t < 20s$). Combined with Fig. 8, the control energy of the aircraft is sufficient and there is no input saturation phenomenon ($t < 20$). However, in twentieth seconds, the actuator fault appears ($\rho = 0.4$). Then, the aircraft is out of control, and the AOA of the aircraft quickly diverges to a higher AOA. According to Fig. 8, it is obvious that the control input is saturated, and the aircraft has no sufficient nose down pitching moment, which means that the aircraft has been locked at the high AOA, and deep stall appears.

As shown in Fig. 7 and Fig. 8, the aircraft does not have enough control power to recover to a small AOA. Hence, it is very urgent to design a viable deep-stall recovery law.

B. DEEP STALL RECOVERY SIMULATION

The prescribed performance functions are chosen as

$$e_u = 10e^{-1.2t} + 2, \quad e_l = -10e^{-0.8t} - 2 \quad (77)$$

The initial conditions of the aircraft are given as $V(0) = 35.45^m/_s$, $h(0) = 3000m$, $\gamma(0) = -45.8^\circ$. The parameters of the controller (27) are $k_{11} = 2, k_{12} = 2, \varepsilon_{\varpi 1} = 0.05, \varepsilon_{11} = 4, \varepsilon_{13} = 4, b_1 = 0.05, \lambda_1 = \frac{3}{5}, k_{21} = 20, k_{22} = 20, \lambda_2 = \frac{3}{5}, \varepsilon_{23} = 2, b_2 = 0.01$. And the parameters for the adaption laws (29) are chosen as $k_{\theta 11} = 5$, $k'_{\theta 11} = 2$, $k_{\theta 12} = 5$, $k'_{\theta 12} = 2$, $k_{\theta 21} = 5$, $k'_{\theta 21} = 2$, $k_{\theta 22} = 5$, $k'_{\theta 22} = 2$. And the simulation results are presented in Fig. 9- Fig. 14.

Meanwhile, the high AOA control law proposed in [29] will be adopted for simulation and comparison, which is given by

$$x_{(i+1)d} = -\left(k_i + \frac{\varepsilon'_i}{2}\right) e_i - \hat{\Theta} \tanh\left(\frac{e_i}{b_i}\right) - \frac{\varepsilon_i}{2} e_i \hat{\theta} S_i^T(Z_i) S_i(Z_i), \quad i = 1, 2 \quad (78)$$

And the adaption laws are defined as

$$\dot{\hat{\theta}} = \sum_{i=1}^{n} \frac{\varepsilon_i r}{2} e_i^2 S_i^T(Z_i) S_i(Z_i) - k_\theta \hat{\theta}$$
$$\dot{\hat{\Theta}} = \beta \sum_{i=1}^{n} e_i \tanh\left(\frac{e_i}{b_i}\right) - k_\Theta \hat{\Theta} \quad (79)$$

where the definition and selection of the controller parameters are the same as those in [29]. And the AOA response curve ($\alpha - ANFC$) and AOA tracking error curve ($e_1 - ANFC$) are given in Figures 9 and 12, respectively.

In Fig. 9, α_c is the AOA command. α denotes the AOA response of the aircraft, which is decided by the controllers (12) and (27). The AOA response curve ($\alpha - ANFC$)

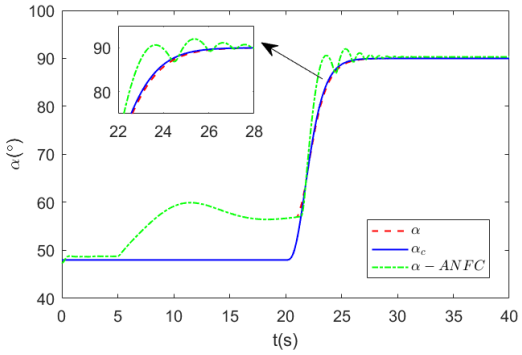

FIGURE 9. Tracking result of α.

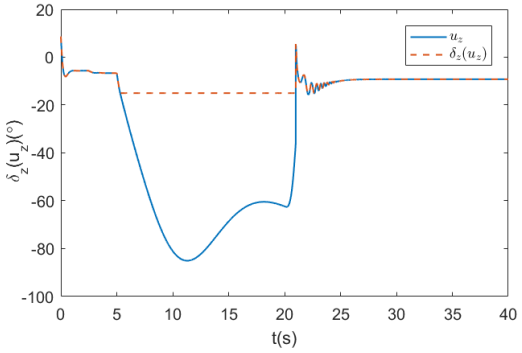

FIGURE 10. Control input signal.

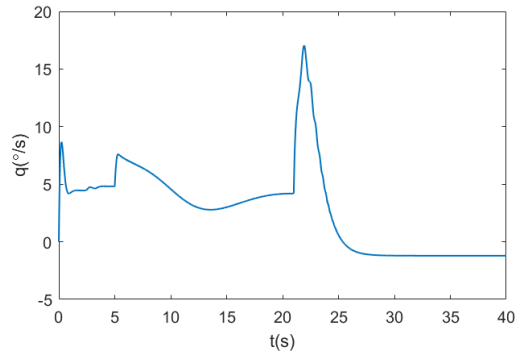

FIGURE 11. Pitching rate response.

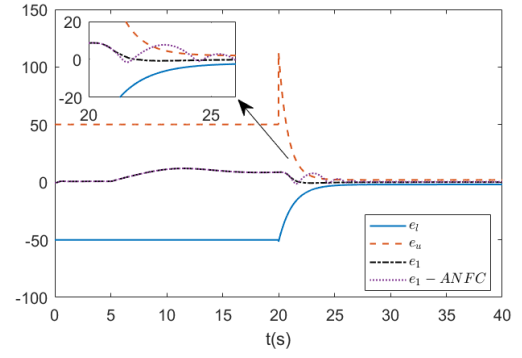

FIGURE 12. Tracking error e_1.

is decided by the controller (78). According to Fig. 9 and Fig. 10, the entire simulation can be divided into three phases:

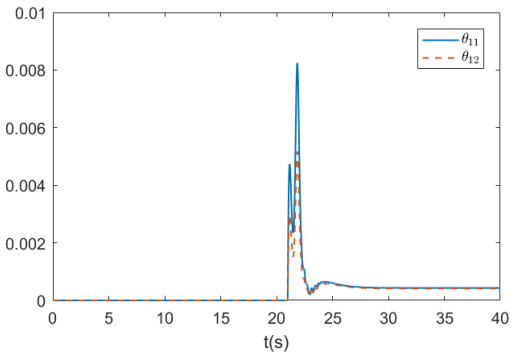

FIGURE 13. Estimations of θ_{11} and θ_{12}.

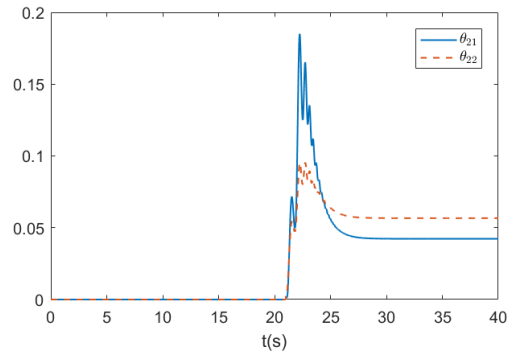

FIGURE 14. Estimations of θ_{21} and θ_{22}.

(1) When $t \in [0, 5)$, the actuator fault does not appear, and $\rho = 1$. In the meantime, the aircraft can follow the AOA command α_c under the flight controller (12).
(2) When $t \in [5, 20)$, the actuator fault occurs ($\rho = 0.44$). Fig. 9 shows that the aircraft is out of control and the angle of attack instantaneously deviates to a higher AOA. Combined with Fig. 10, it can be found that the control output is saturated, and the aircraft has no excess control energy to reduce the AOA. Hence, the AOA of the aircraft has been locked, and deep stall appeared.
(3) When $t \in [20, 40)$, the deep-stall recovery control scheme (27) has been activated. First, by analyzing the deep-stall AOA and the bifurcation analysis results in Fig. 3 - Fig. 6, the actuator fault is estimated. Further, according to the bifurcation analysis results, the maximum stable AOA that the aircraft can track is analyzed. Finally, according to the maximum stable AOA, a suitable high AOA tracking command is designed, which is given in Fig. 9.

According to the AOA response curve (α) in Fig. 9, the designed controller (27) can make the aircraft follow the high AOA command (α_c) according to the prescribed performance ($20 \leq t < 40$). However, the AOA response curve ($\alpha - ANFC$) in Fig. 9 show that the control law designed in [29] can not guarantee the better transient performance in the presence of actuator failure. And tracking error curves in Fig. 12 can also confirm the above discussion.

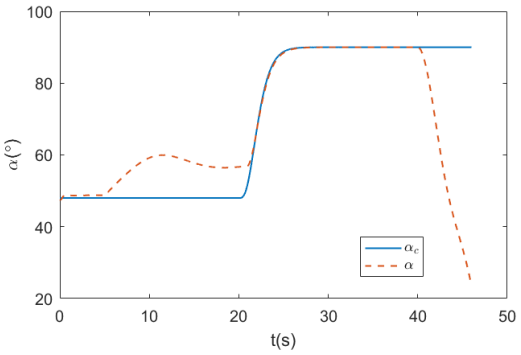

FIGURE 15. Complete AOA response process.

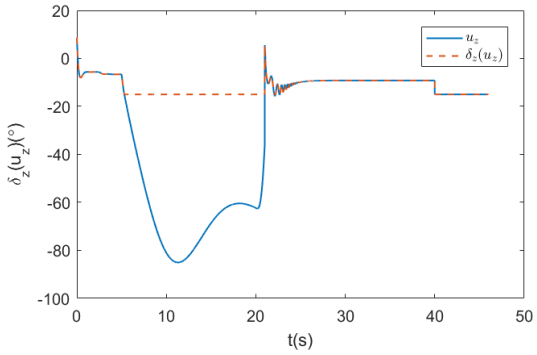

FIGURE 16. Complete control input.

According to Fig. 12, the tracking error e_1 can meet the preset performance requirements well. Fig. 13 and Fig. 14 show that estimated values of θ_{11}, θ_{12}, θ_{21}, and θ_{22} converge to a reasonable bound.

In Fig. 9, the aircraft has pitched up to the specified AOA at the 40th second. At this time, the aircraft will be disconnected from the controller (27) and the pilot will immediately put the rod, so that the aircraft will achieve the deep-stall recovery. And the complete process is given in Fig. 15 and Fig. 16.

Comparing the control methods in this paper with those in [29], it can be concluded that the combination of finite-time control and prescribed performance method can effectively improve the transient performance of aircraft maneuvering at high AOA, especially in the case of actuator failure. Meanwhile, according to Fig. 12 and Fig. 16, better control performance requires higher control energy. Fig. 16 shows high control performance leads to serious input saturation. Hence, the balance between control performance and the effects of actuator fault should be considered. In the design of deep-stall recovery scheme, appropriate prescribed performance functions should be selected according to the failure degree of the actuator.

VI. CONCLUSION

In this paper, the problem of deep-stall recovery has been studied for the aircraft without ''spoon-like'' longitudinal torque characteristics. Meanwhile, the effects of actuator fault on deep stall have been analyzed through the bifurcation method. Considering that the studied aircraft is longitudinally unstable, existing deep-stall recovery methods are difficult to use directly. The bifurcation analysis method has been used to assist in the design of a finite-time prescribed performance deep-stall recovery law, and simulation results showed that this method can achieve satisfactory deep-stall recovery performance. In the future, we will consider further researches in the following areas. First, actuator fault identification and diagnostic technique will be studied for high AOA flight to provide more information for deep-stall recovery. Secondly, we will consider the control distribution of the canard and the thrust vector, which can provide more control energy for the deep-stall recovery.

REFERENCES

[1] R. C. Montgomery and M. T. Moul, ''Analysis of deep-stall characteristics of T-tailed aircraft configurations and some recovery procedures,'' *J. Aircr.*, vol. 3, no. 6, pp. 562–566, 1966.
[2] R. B. Green and R. A. M. Galbraith, ''Dynamic recovery to fully attached aerofoil flow from deep stall,'' *AIAA J.*, vol. 33, no. 8, pp. 1433–1440, Aug. 1995.
[3] M. R. Visbal, ''Numerical investigation of deep dynamic stall of a plunging airfoil,'' *AIAA J.*, vol. 49, no. 10, pp. 2152–2170, Oct. 2011.
[4] O. I. Iloputaife, ''Design of deep stall protection for the C-17A,'' *J. Guid., Control, Dyn.*, vol. 20, no. 4, pp. 760–767, Jul. 1997.
[5] J. H. Xin and C. Liu, ''Characteristics of aircraft deep-stall recovery,'' *Flight Dyn.*, no. 2, pp. 44–49, 1993.
[6] K. G. Gousnan, J. C. Juang, and R. C. Loschke, ''Aircraft deep stall analysis and recovery,'' in *Proc. AIAA*, 1991, Paper 91–2888, pp. 385–394.
[7] Y. L. Chen, H. L. Shen, and C. Liu, ''Analysis and control of aircraft deep stall recovery characteristics,'' *J. Nanjing Univ. Aeronaut. Astromautics*, vol. 39, no. 4, pp. 435–439, 2007.
[8] S. A. Snell, ''Nonlinear dynamic-inversion flight control of supermaneuverable aircraft,'' Ph.D. dissertation, Univ. Minnesota, Minneapolis, MN, USA, 1991.
[9] W. H. Hui and M. Tobak, ''Bifurcation analysis of aircraft pitching motions about large mean angles of attack,'' *J. Guid., Control, Dyn.*, vol. 7, no. 1, pp. 113–122, Jan. 1984.
[10] J. Rankin, E. Coetzee, B. Krauskopf, and M. Lowenberg, ''Bifurcation and stability analysis of aircraft turning on the ground,'' *J. Guid., Control, Dyn.*, vol. 32, no. 2, pp. 500–511, Mar. 2009.
[11] A. K. Khatri and N. K. Sinha, ''Aircraft maneuver design using bifurcation analysis and nonlinear control techniques,'' *J. Guid., Control, Dyn.*, vol. 35, no. 5, pp. 1435–1449, 2012.
[12] J. V. Carroll and R. K. Mehra, ''Bifurcation analysis of nonlinear aircraft dynamics,'' *J. Guid., Control, Dyn.*, vol. 5, no. 5, pp. 529–536, Sep. 1982.
[13] A. K. Khatri, J. Singh, and N. K. Sinha, ''Aircraft maneuver design using bifurcation analysis and sliding mode control techniques,'' *J. Guid., Control, Dyn.*, vol. 35, no. 5, pp. 1435–1449, Sep. 2012.
[14] N. Baghdadi, M. H. Lowenberg, and A. T. Isikveren, ''Analysis of flexible aircraft dynamics using bifurcation methods,'' *J. Guid., Control, Dyn.*, vol. 34, no. 3, pp. 795–809, May 2011.
[15] C. P. Bechlioulis and G. A. Rovithakis, ''Robust adaptive control of feedback linearizable MIMO nonlinear systems with prescribed performance,'' *IEEE Trans. Autom. Control*, vol. 53, no. 9, pp. 2090–2099, Oct. 2008.
[16] A. K. Kostarigka and G. A. Rovithakis, ''Adaptive dynamic output feedback neural network control of uncertain MIMO nonlinear systems with prescribed performance,'' *IEEE Trans. Neural Netw. Learn. Syst.*, vol. 23, no. 1, pp. 138–149, Jan. 2012.
[17] J. Na, ''Adaptive prescribed performance control of nonlinear systems with unknown dead zone,'' *Int. J. Adapt. Control Signal Process.*, vol. 27, no. 5, pp. 426–446, May 2013.
[18] C. P. Bechlioulis, Z. Doulgeri, and G. A. Rovithakis, ''Neuro-adaptive force/position control with prescribed performance and guaranteed contact maintenance,'' *IEEE Trans. Neural Netw.*, vol. 21, no. 12, pp. 1857–1868, Dec. 2010.

[19] Y. Li, S. Tong, L. Liu, and G. Feng, "Adaptive output-feedback control design with prescribed performance for switched nonlinear systems," *Automatica*, vol. 80, pp. 225–231, Jun. 2017.

[20] H. Liu, S. Li, J. Cao, G. Li, A. Alsaedi, and F. E. Alsaadi, "Adaptive fuzzy prescribed performance controller design for a class of uncertain fractional-order nonlinear systems with external disturbances," *Neurocomputing*, vol. 219, pp. 422–430, Jan. 2017.

[21] S. Yu, X. Yu, B. Shirinzadeh, and Z. Man, "Continuous finite-time control for robotic manipulators with terminal sliding mode," *Automatica*, vol. 41, no. 11, pp. 1957–1964, Nov. 2005.

[22] F. Amato and M. Ariola, "Finite-time control of discrete-time linear systems," *IEEE Trans. Autom. Control*, vol. 50, no. 5, pp. 724–729, May 2005.

[23] F. Amato, M. Ariola, and C. Cosentino, "Finite-time control of discrete-time linear systems: Analysis and design conditions," *Automatica*, vol. 46, no. 5, pp. 919–924, May 2010.

[24] J. Cheng, J. H. Park, and Y. Liu, "Finite-time H∞ fuzzy control of nonlinear Markovian jump delayed systems with partly uncertain transition descriptions,"' *Fuzzy Sets Syst.*, vol. 314, pp. 99–115, 2017.

[25] Y. Shen, "Finite-time control of linear parameter-varying systems with norm-bounded exogenous disturbance," *J. Control Theory Appl.*, vol. 6, no. 2, pp. 184–188, May 2008.

[26] N. Wang, C. Qian, J.-C. Sun, and Y.-C. Liu, "Adaptive robust finite-time trajectory tracking control of fully actuated marine surface vehicles," *IEEE Trans. Control Syst. Technol.*, vol. 24, no. 4, pp. 1454–1462, Jul. 2016.

[27] M. Goman, G. Zagainov, and A. Khramtsovsky, "Application of bifurcation methods to nonlinear flight dynamics problems," *Progr. Aerosp. Sci.*, vol. 33, nos. 9–10, pp. 539–586, Jan. 1997.

[28] Y. Zhong, Y. Zhang, W. Zhang, J. Zuo, and H. Zhan, "Robust actuator fault detection and diagnosis for a quadrotor UAV with external disturbances," *IEEE Access*, vol. 6, pp. 48169–48180, 2018.

[29] D. Wu, M. Chen, and H. Gong, "Adaptive neural flight control for an aircraft with time-varying distributed delays," *Neurocomputing*, vol. 307, pp. 130–145, Sep. 2018.

[30] C. P. Bechlioulis and G. A. Rovithakis, "Prescribed performance adaptive control for multi-input multi-output affine in the control nonlinear systems," *IEEE Trans. Autom. Control*, vol. 55, no. 5, pp. 1220–1226, May 2010.

[31] H. Yue and J. Li, "Adaptive fuzzy tracking control for a class of nonlinear systems with unknown distributed time-varying delays and unknown control directions," *Iranian J. Fuzzy Syst.*, vol. 11, no. 1, pp. 1–25, 2014.

[32] M. Chen, S. S. Ge, and B. How, "Robust adaptive neural network control for a class of uncertain MIMO nonlinear systems with input nonlinearities," *IEEE Trans. Neural Netw.*, vol. 21, no. 5, pp. 796–812, May 2010.

[33] M. Chen and S. S. Ge, "Adaptive neural output feedback control of uncertain nonlinear systems with unknown hysteresis using disturbance observer," *IEEE Trans. Ind. Electron.*, vol. 62, no. 12, pp. 7706–7716, Dec. 2015.

[34] Z. Liu, B. Chen, and C. Lin, "Adaptive neural backstepping for a class of switched nonlinear system without strict-feedback form," *IEEE Trans. Syst., Man, Cybern., Syst.*, vol. 47, no. 7, pp. 1315–1320, Jul. 2017.

[35] Q. Yang and M. Chen, "Adaptive neural prescribed performance tracking control for near space vehicles with input nonlinearity," *Neurocomputing*, vol. 174, pp. 780–789, Jan. 2016.

[36] C. Qian and W. Lin, "Non-Lipschitz continuous stabilizers for nonlinear systems with uncontrollable unstable linearization," *Syst. Control Lett.*, vol. 42, no. 3, pp. 185–200, Mar. 2001.

[37] Y. Sun, B. Chen, C. Lin, and H. Wang, "Finite-time adaptive control for a class of nonlinear systems with nonstrict feedback structure," *IEEE Trans. Cybern.*, vol. 48, no. 10, pp. 2774–2782, Oct. 2018.

[38] B. Chen, X. P. Liu, S. S. Ge, and C. Lin, "Adaptive fuzzy control of a class of nonlinear systems by fuzzy approximation approach," *IEEE Trans. Fuzzy Syst.*, vol. 20, no. 6, pp. 1012–1021, Dec. 2012.

[39] H. Wang, X. Liu, K. Liu, and H. R. Karimi, "Approximation-based adaptive fuzzy tracking control for a class of nonstrict-feedback stochastic nonlinear time-delay systems," *IEEE Trans. Fuzzy Syst.*, vol. 23, no. 5, pp. 1746–1760, Oct. 2015.

[40] Q. Zhou, L. Wang, C. Wu, H. Li, and H. Du, "Adaptive fuzzy control for nonstrict-feedback systems with input saturation and output constraint," *IEEE Trans. Syst., Man, Cybern., Syst.*, vol. 47, no. 1, pp. 1–12, Jan. 2017.

[41] A. A. Khater, A. M. El-Nagar, M. El-Bardini, and N. El-Rabaie, "A novel structure of actor-critic learning based on an interval type-2 TSK fuzzy neural network," *IEEE Trans. Fuzzy Syst.*, to be published.

[42] Y. Gao, J. Liu, Z. Wang, and L. Wu, "Interval type-2 FNN-based quantized tracking control for hypersonic flight vehicles with prescribed performance," *IEEE Trans. Syst., Man, Cybern., Syst.*, to be published.

[43] M. Gao and J. Yao, "Finite-time H∞ adaptive attitude fault-tolerant control for reentry vehicle involving control delay," *Aerosp. Sci. Technol.*, vol. 79, pp. 246–254, Aug. 2018.

[44] M. Wang, B. Chen, X. Liu, and P. Shi, "Adaptive fuzzy tracking control for a class of perturbed strict-feedback nonlinear time-delay systems," *Fuzzy Sets Syst.*, vol. 159, no. 8, pp. 949–967, Apr. 2008.

[45] M. Chen, G. Tao, and B. Jiang, "Dynamic surface control using neural networks for a class of uncertain nonlinear systems with input saturation," *IEEE Trans. Neural Netw. Learn. Syst.*, vol. 26, no. 9, pp. 2086–2097, Sep. 2015.

[46] Q. Shen, B. Jiang, and V. Cocquempot, "Adaptive fault-tolerant backstepping control against actuator gain faults and its applications to an aircraft longitudinal motion dynamics," *Int. J. Robust Nonlinear Control*, vol. 23, no. 15, pp. 1753–1779, 2013.

[47] S.-H. Yoon, Y.-D. Kim, and S.-H. Park, "Constrained adaptive backstepping controller design for aircraft landing in wind disturbance and actuator stuck," *Int. J. Aeronaut. Space Sci.*, vol. 13, no. 1, pp. 74–89, Mar. 2012.

[48] J. Chen, S. L. Zhou, and Z. Song, "Hypersonic aircraft dynamic surface adaptive backstepping control system design based on uncertainty," *J. Astronaut.*, vol. 31, no. 11, pp. 2550–2556, 2010.

[49] K. Vladislav and P. C. Murphy, "Estimation of aircraft nonlinear unsteady parameters from wind tunnel data," in *Proc. AIAA Atmos. Flight Mech. Conf. Exhibit*, 2001. [Online]. Available: https://arc.aiaa.org/doi/abs/10.2514/6.2001-4016

DAWEI WU received the Ph.D. degree in navigation, guidance, and control from the College of Automation Engineering, Nanjing University of Aeronautics and Astronautics, Nanjing, China, in 2019. He is currently a Lecturer of the College of Energy and Electrical Engineering, Hohai University, Nanjing. His current research interests include nonlinear system control and flight control.

MOU CHEN (Member, IEEE) received the B.S. degree in material science and engineering and the Ph.D. degree in control theory and control engineering from the Nanjing University of Aeronautics and Astronautics (NUAA), Nanjing, China, in 1998 and 2004, respectively. He was an Academic Visitor with the Department of Aeronautical and Automotive Engineering, Loughborough University, Loughborough, U.K., from November 2007 to February 2008. From June 2008 to September 2009, he was a Research Fellow with the Department of Electrical and Computer Engineering, National University of Singapore, Singapore. From May 2014 to November 2014, he was a Senior Academic Visitor with the School of Electrical and Electronic Engineering, The University of Adelaide, Adelaide, SA, Australia, for seven months. He is currently a Full Professor with the College of Automation Engineering, NUAA. His current research interests include nonlinear system control, intelligent control, and flight control.

HUI YE was born in Zhenjiang, China, in 1986. He received the B.S. degree in flight vehicle propulsion engineering and the Ph.D. degree in control theory and control engineering from the Nanjing University of Aeronautics and Astronautics (NUAA), Nanjing, China, in 2007 and 2016, respectively. He is currently a Lecturer of the School of Electronics and Information, Jiangsu University of Science and Technology (JUST), Zhenjiang, China. His current research interests include nonlinear control systems, flight control, and underwater vehicle control.